Investigation of Concrete Mixtures to Reduce Differential Shrinkage Cracking in Composite Bridges

By

Douglas A. Nelson

Thesis submitted to the Faculty of the Virginia Polytechnic Institute and State University in partial fulfillment of the requirements for the degree of

Master of Science

In

Civil Engineering

Carin L. Roberts-Wollmann, Chair

Thomas E. Cousins

Zachary C. Grasley

David W. Mokarem

September 19, 2013

Blacksburg, Virginia

Concrete Bridge Decks, Differential Shrinkage, Rapid Construction, Tensile Creep

Investigation of Concrete Mixtures to Reduce Differential Shrinkage Cracking in Composite Bridges

ABSTRACT

Douglas A. Nelson

The objective of the research presented in this thesis was to develop a concrete bridge deck topping mixture that resists the effects of differential shrinkage by decreasing shrinkage and increasing creep. . In addition, the amount of tensile creep that concrete experiences under long-term tensile stresses were quantified and compared to compressive creep values in order to gain a better understanding of how concrete behaves under tension. Test results show that the amount of tensile creep exceeded compressive creep by a factor of 2-5.

Various shrinkage and creep models were compared against test data in order to quantify results and determine the best model to use for the mixes examined during this research project. Data analysis revealed that the AASHTO time dependent effects (shrinkage and creep) models outperformed the other models used in this research project. Other material property data including compressive strength, splitting tensile strength, Young's modulus of elasticity, and unrestrained shrinkage was also collected to compare against a common bridge deck topping mix to ensure that the mixes used in this research project are suitable for use in the field.

A parametric study utilizing the Age Adjusted Effective Modulus (AAEM) method was performed which showed that the most important factor in reducing tensile stresses was to decrease the amount of shrinkage experienced by the concrete bridge deck topping mixture.

Three concrete mixtures, one included saturated lightweight aggregates (SLWA), one including ground granulated blast furnace slag (GGBFS), and one incorporating both were tested. Preliminary results show that the inclusions of SLWA into a concrete mixture reduced shrinkage by 25% and overall tensile stress by 38%.

ACKNOWLEDGEMENTS

I would like to thank Dr. Carin Roberts-Wollmann for her support and patience during the course of this research project. I have learned more during the last two years than I thought possible and am very grateful for the opportunity that has been given to me.

I would also like to thank Dr. Thomas Cousins, Dr. Zachary Grasley, and Dr. David Mokarem for their insights and assistance with this research project.

I would like to thank Brett Farmer and Dennis Huffman for all of their help in the structures lab during my testing. They are an invaluable resource and this project would not have been possible without them.

I would like to thank Lucas Cotterell and all of my fellow graduate students for their help during this project. I would not have been able to complete this without them.

Finally, I am very grateful to my wife as well as my family for their unfailing support and encouragement, both mentally and financially during the last two years.

All of the photos are by the author.

Contents

List of Tables

List of Figures

CHAPTER 1: INTRODUCTION

Durability of bridges has always been a topic of concern due to the high cost of repairing and rehabilitating deteriorated areas of bridge decks. In areas where ice and snow are common during the winter months, de-icing salts and chemicals are used to ensure the safety of the public. However, these materials can cause serious problems in bridge decks as the chlorides from the salts penetrate the concrete and cause corrosion in the top layer of steel reinforcement bars (rebar) in the deck. Corrosion is an expansive chemical reaction which causes cracking, spalling, delamination, and overall deterioration of the concrete above the rebar. Over time, the bridge deck will become increasingly unusable and eventually require rehabilitation (a process in which the top layer of concrete is milled off, the rebar is cleaned by sandblasting the corrosion products off, and a fresh layer of concrete is placed above the rebar) which is an expensive and time-consuming process, or complete replacement.

Cracking in a bridge deck provides an easy ingress for chlorides to reach the rebar and accelerate the deterioration process. Many short to medium span bridges are constructed by placing a pre-cast concrete girder in place and placing a cast-in-place deck on top. The concrete girder is cast off-site at a precast yard and in most cases has undergone most of its time-dependent deformations while at the precast yard. The girder-deck system is designed to be composite (i.e. acting as one unit) by means of reinforcement tying the girder and deck together. During placement the deck will shrink and creep but will be partially restrained by the girder, resulting in differential shrinkage and creep. As a result, the deck will develop tensile stresses which in many cases will exceed the concrete's tensile strength and cause cracking.

These cracks will accelerate the deterioration process and are a major problem in the durability of a bridge.

This research project will attempt to mitigate differential shrinkage through the addition of saturated lightweight aggregates and supplementary cementitious materials in order to create a bridge deck topping mix which will experience reduced shrinkage and increased creep. Reducing shrinkage will result in reduced tensile stresses due to shrinkage restraint. Increasing creep will result in increased dissipation of tensile stresses as the concrete creeps in the direction of stress. In addition, the amount of tensile creep that concrete experiences under long-term tensile stresses will be quantified and compared to compressive creep values in order to gain a better understanding of how concrete behaves under tension. Various shrinkage and creep models will be compared against test data in order to quantify results and determine the best model to use for the mixes examined during this research project. Other material property data including compressive strength, splitting tensile strength, Young's modulus of elasticity, and unrestrained shrinkage will also be collected to compare against a common bridge deck topping mix to ensure that the mixes used in this research project are suitable for use in the field.

CHAPTER 2: LITERATURE REVIEW

This literature review covers various topics related to the issue of differential shrinkage in bridge decks, including shrinkage, creep (both tensile and compressive), and methods for reducing shrinkage such as the addition of saturated lightweight aggregates and supplementary cementitious materials.

2.1 Shrinkage

As concrete ages, it undergoes a change in volume, known as shrinkage. If concrete were unrestrained, this volumetric change would have no effect. However, since concrete is generally restrained in some way, stresses will develop over time which can reduce the durability of the material. Concrete is generally strong in compression but weak in tension. The stresses which develop due to restrained shrinkage are generally tensile in nature. This may eventually cause cracking in the material, reducing its lifespan. Concrete undergoes shrinkage throughout its lifecycle due to several different mechanisms, which are discussed hereafter. (Kosmatka, Kerkhoff et al. 2002)

2.1.1 Chemical Shrinkage

Chemical shrinkage occurs during the chemical process of hydration. As the cement reacts with the liquids in the concrete mixture, the total volume of the concrete paste is reduced. The total volume of hydrated cement paste is smaller than the total volume of cement and water prior to the reaction. This process continues until all of the cement is fully hydrated, assuming there is sufficient water to allow for complete hydration. (Kosmatka, Kerkhoff et al. 2002)

2.1.2 Autogenous Shrinkage

Autogenous shrinkage is the macroscopic counterpart to chemical shrinkage. As the cement hydrates, a change in volume can be observed. The volume reduction due to autogenous shrinkage is smaller than that observed due to chemical shrinkage due to the fact that the paste structure has hardened and become rigid. Autogenous shrinkage can be mitigated by the external application of water to the structure (such as the addition of saturated lightweight aggregates). If there is no external water available, hydration of the cement paste will consume pore fluid within the concrete, resulting in self desiccation and reduction in total volume. Autogenous shrinkage is negligible in concrete mixes with a water/cement ratio of 0.42 or higher due to the large amounts of water available for hydration within the pore fluid. The lower the water/cement ratio, the larger the role that autogenous shrinkage will play in the overall shrinkage experienced by the concrete. (Kosmatka, Kerkhoff et al. 2002)

2.1.3 Plastic Shrinkage

Plastic shrinkage refers to volume change experienced by concrete shortly after placement, prior to initial set/hardening. It is caused by rapid evaporation of water from the surface of the concrete in excess of the bleeding rate. The loss of water will cause cracking on the surface of the material that resemble “tearing”. Plastic shrinkage cracking can be minimized by providing evaporation protection to the material via wet burlap, misting, or other means of reducing evaporation. (Kosmatka, Kerkhoff et al. 2002)

2.1.4 Drying Shrinkage

Drying shrinkage is caused by external evaporation of moisture from concrete. It differs from autogenous shrinkage in that rather than the water within the concrete being consumed, the

water is leaving the system due to evaporation. Drying shrinkage is the dominant mode in concrete slabs (or structures with slab-like volume/surface ratio) with plentiful water (water/cement ratio greater than ~0.41). This process can continue for a number of years, depending on the shape and volume/surface ratio of the concrete structure. However, within the first about 11 months, tests have shown that approximately 90 percent of shrinkage had taken place, although this number is subject on many other factors. (Kosmatka, Kerkhoff et al. 2002)

2.2 Differential Shrinkage

2.2.1 Causes of Differential Shrinkage

Differential shrinkage occurs when two different materials (in most cases, a cast-in-place bridge deck topping and a precast girder) are combined to act in a composite fashion. The precast girder component will generally be shipped from a precast yard after having been aged for some amount of time. Since the precast component has been aged, it will have already undergone some amount of shrinkage. The cast-in-place (CIP) topping will shrink considerably, but will be restrained by the precast section. The resulting differential shrinkage causes stresses in the composite section which are mainly tensile in the CIP topping. (Silfwerbrand 1997)

2.2.2 Effects of Differential Shrinkage

The resulting tensile stresses from differential shrinkage in combination with stresses from live and dead loadings can cause cracking in the bridge deck topping. This allows for the ingress of detrimental materials such as moisture and deicing salts, causing further deterioration due to corrosion of reinforcement. In the absence of remedial action, this can lead to serious issues

with the long-term integrity of the structure, including concrete spalling, delaminations, and eventual requirement of total deck rehabilitation or replacement.

2.2.3 Mitigation of Differential Shrinkage

The effects of differential shrinkage can be reduced in two ways. The first way is to reduce shrinkage. This will reduce the tensile stresses built up in the cross section. The second way is to increase creep. As the structure creeps due to tensile stress caused by differential shrinkage, the material will relax and dissipate some amount of the tensile stress.

2.3 Creep

Creep in concrete is often seen as an undesirable effect, however, in the case of differential shrinkage it can be beneficial. Concrete will creep in tension due to the tensile stresses caused by differential shrinkage. This creep effect serves to relax these stresses and reduce the likelihood of the concrete cracking due to the aforementioned stresses. (Kosmatka, Kerkhoff et al. 2002)

2.3.1 Drying Creep

Drying creep can be observed in a specimen when it is subjected to drying as well as a sustained external load. The total deformation of the specimen differs from the superimposed total of drying shrinkage strain and delayed strain (creep) due to the external load. The observed difference between the measured strains and strains due to superimposed effects may be interpreted as drying creep. (Pickett 1942)

2.3.2 Compressive Creep

Creep is defined as an increase in strain over time due to a constant stress. When a concrete cross-section/structure is loaded, it experiences two types of strain. The first is elastic strain due to instantaneous deformation as per Hooke's law. The second type (creep) is a time-dependent deformation that begins immediately and continues for as long as the concrete experiences load. This amount of creep is reliant on the amount of load, the capability of the concrete to handle the load, and the length of time that the load is applied to the cross-section. (Kosmatka, Kerkhoff et al. 2002)

2.3.3 Tensile Creep

In his paper on tensile basic creep, Østergaard (2001) states that the early age basic tensile creep response of concrete has not been extensively examined. Most of the work done on basic creep has been focused on compressive creep of mature concrete. However, information about tensile creep behavior at early ages is important for estimating the possibility of cracking due to shrinkage and thermal stresses. Østergaard states that prior work done in the field found that tensile and compressive creep amounts are comparative and that specific creep response was found to be linear below a stress/strength ratio of 60%. He concludes that experiments indicated that the creep rate after a short initial time after loading is constant regardless of age at loading given constant initial stress/strength ratio. However, a caveat is included that his article only represents limited amounts of experimental evidence and more experiments are needed for confirmation of his results.

Bissonnette (1995) states that the majority of the work on tensile creep tends to indicate that the tensile creep component is not negligible when concrete is allowed to dry under load

(drying creep) and that the influence of most basic parameters, such as water to cement (w/c) ratio has not been extensively studied. Bissonnette found that the main parameters effecting tensile creep were the water to cement ratio and the age of the concrete at loading.

Rossi (2013) investigated the relationship between tensile and compressive creep and found that compressive and tensile creep seem to be equivalent under drying conditions (i.e. specimens open to air). They noticed some difference between these curves but attributed it to natural scattering due to the inherent variability of the material. It is further stated that under tensile loading, cracks created on the specimen surface due to shrinkage under drying conditions can propagate under tensile stresses and induce large amounts of strain. These cracks will accelerate the rate of drying shrinkage due to an increased volume/surface ratio and lead to an increase in tensile strain.

Nahas et al. (2008) carried out an experimental study of tensile creep in concrete for different loading levels. During their three day tests, they found that tensile drying creep compliance was the same as compressive drying creep compliance. Due to other similarities, they concluded that the mechanisms for compressive and drying tensile creep were the same.

Poston et al. (1998) carried out tensile creep testing on unsealed concrete specimens and found that their specimens fractured when subjected to long term loading at 40% of tested tensile capacity and thus reduced their long term loading levels to 20% of their tensile capacity. They produced the table presented in Figure 1 detailing various ratios of tensile to compressive creep for 12 different materials. They state that tensile creep can be generalized as approximately 1.2 times higher than compressive creep for a concrete material.

Table 15
Ratio of Tensile to Compressive Specific Creep[1]

Material No.	Ratio
1	1.06
2	1.26
3	0.81
4	1.13
5	47.81
6	0.90
7	0.92
8	1.77
9	1.07
10	0.04
11	1.64
12	≈0

[1] Specific creep values at 1 year.

Figure 1 - Ratio of Tensile to Compressive Specific Creep. (Poston et al., 1998)

2.4 Methods of Improving Concrete Time Dependent Properties

The scope of this research project includes two main thrusts aimed towards creating an improved bridge deck topping concrete mix. The first involves the use of saturated lightweight aggregates (SLWA) which provide internal curing in order to reduce shrinkage and self-desiccation. A side effect of using lightweight fine aggregates is that strength, unit weight, and modulus of elasticity are reduced, resulting in increased creep which is beneficial for increasing the amount of tensile stress relaxation which occurs under differential shrinkage. The second

uses ground granulated blast furnace slag (GGBFS) cement as a partial replacement for Portland cement concrete (PCC) as research has shown that slag cement results in reduced shrinkage and increased strength. When used together, the increased strength associated with GGBFS is expected to counteract the reduction in strength caused by the inclusion of SLWA into the concrete mix.

In their article entitled "Effect of Material Properties on Cracking in Bridge Decks", Schmitt and Darwin (1999) conclude that cracking increases with increasing values of concrete slump, percentage volume of water and cement, water content, cement content, and compressive strength. These results suggest that decreasing w/c ratio and compressive strength (both of these factors are present in the proposed SLWA mixture) will have a beneficial effect in decreasing cracking in a monolithic bridge deck.

2.4.1 Saturated Lightweight Aggregates (SLWA)

Henkensiefken et al. (2009) examined mortar systems with different volumes of SLWA under sealed and unsealed conditions. They found that the internal curing provided by SLWA depended on three main factors – firstly, the volume of water available for internal curing, secondly, the ability of the water to leave the SLWA when needed, and thirdly, the distribution of the SLWA so that it is well dispersed and its water can readily travel to all of the sections in the paste where it is needed. They found that there was a critical level of SLWA at which shrinkage began to decrease. In the unsealed condition, they found that (as seen in Figure 2) replacement volumes less than 14.3% were similar (time of cracking ~2 days) to that of plain mixtures that did not utilize SLWA. When a larger (23.7%) volume was used, time to cracking was increased to about 8 days. With a further increase to 29.3% replacement volume, cracking

was delayed to 14 days. Finally, with a mixture utilizing 33.3% replacement volume, the specimens did not crack during the 14 day testing period and showed little shrinkage strain.

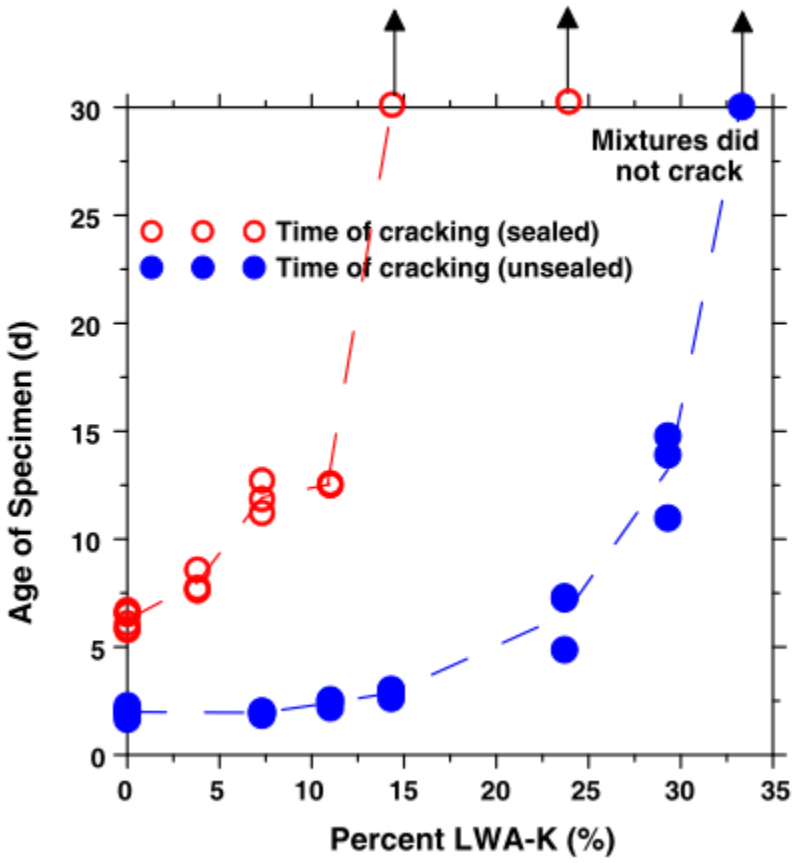

Figure 2 - Time of cracking in LWA-K mixtures plotted as a function of replacement volume. Henkensiefken, 2009

Zha, et al. (2009) investigated the influence of varying amounts of SLWA on internal curing of concrete. They found that the concrete including SLWA exhibited reduction in autogenous and drying shrinkage when compared to a reference concrete which did not incorporate SLWA. They tested four mixes, using 0%, 10%, 30%, and 50% replacement of fine aggregates with SLWA and monitored autogenous and drying shrinkage over the first 28 days of the lifespan of

the material. The specimens used for testing were 100 mm x 100 mm x 515 mm shrinkage prisms. Shrinkage values were determined by measuring length change of sealed and unsealed specimens starting at 24 hours after placement. The results of their testing are shown in Figures 3 and 4.

The legend can be interpreted as follows:

A0 = 0% replacement of FA with SLWA

A10 = 10% replacement of FA with SLWA

A30 = 30% replacement of FA with SLWA

A50 = 50% replacement of FA with SLWA

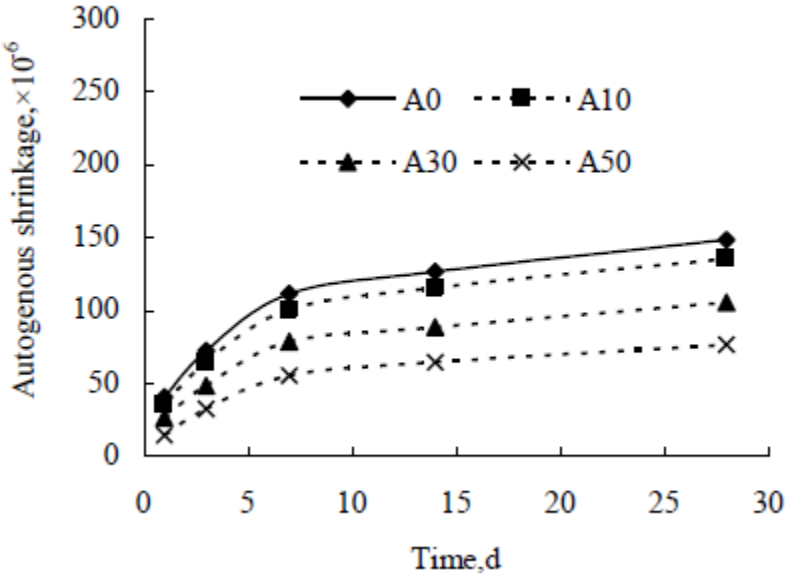

Figure 3 - Effect of saturated lightweight aggregate on autogenous shrinkage. Zha, et al., 2009

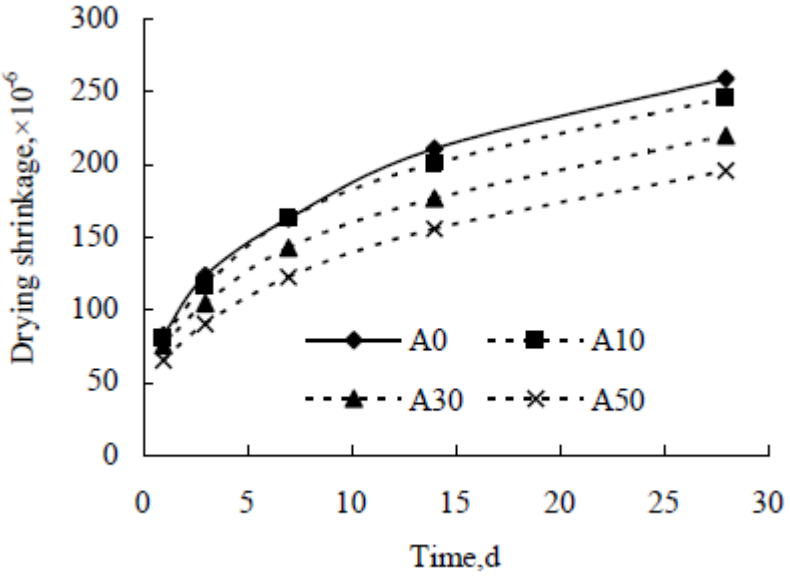

Figure 4 - Effect of saturated lightweight aggregate on drying shrinkage. Zha, et al., 2009

From these results it can be seen that the addition of SLWA to a mix has reduced both autogenous and differential shrinkage to varying degrees depending on the amount of SLWA used in the concrete mix.

2.4.2 Supplementary Cementitious Materials (Slag)

One undesired side effect of the addition of SLWA to concrete is reduction in strength. Slag cement used as a partial replacement of Portland cement has been shown to increase compressive strength of concrete mixes. Wang, et al. (1995) states that benefits of using slag cement in a concrete mix include high strength, rapid hardening, and large strength gain in the long term. In addition, the water requirements of slag cement is lower than that of normal Portland cement, enabling greater workability while reducing w/c ratios which will have the effect of reducing drying shrinkage rate.

The literature provides conflicting information on the effects of the addition of slag cement on shrinkage. In their review titled "The Effect of GGBFS on the Drying Shrinkage of Concrete – A Critical Review of the Literature" (Hooton, Stanish et al. 2004), the authors state that while individual data in the literature shows higher drying shrinkage in mixes containing GGBFS, there are other factors which could explain the increase other than the addition of slag cement. The data shows that the drying shrinkage for concretes containing GGBFS was on average 2.9% higher than concretes without slag – however, the authors determine that the only parameter of the mix design that would have had an influence on the drying shrinkage was the total aggregate volume. Any increase in drying shrinkage of the slag concrete was typically reduced with increasing aggregate content. Most of the mixes reviewed with GGBFS had reduced aggregate content compared to those only containing Portland cement due to slag's lower density when slag was used as a replacement on an equal mass basis. Once the slag amount is corrected, the shrinkage becomes equal to that seen in Portland cement concretes. In addition, the data, although limited, shows that concrete containing GGBFS appears to have reduced restrained shrinkage cracking compared to concretes without slag. If repeatable, this would have positive connotations for bridge deck toppings including slag cement.

Past research at Virginia Tech has shown that cement mixtures with partial replacement of Portland cement with ground granulated blast furnace slag (GGBFS) has yielded reduced shrinkage over time. Work was done during summer of 2011 by Menkulasi, Mercer, and Vaanjilnorov (2011) comparing several different mixes incorporating fly ash and GGBFS as a partial replacement for Portland cement to determine which admixture was best suited for a bridge deck topping with reduced shrinkage. Vaanjilnorov (2011) states that "At 100 days the

normal weight slag and normal weight fly ash concrete mixes had close range of shrinkage, 483 με and 466 με respectively". These results do not take into account early age shrinkage results during the first 7 days which showed that the GGBFS cement mix had reduced shrinkage compared to the fly ash mixture.

In addition, work was done by Mokarem (2002) regarding the addition of fly ash and GGBFS into A4/A5 concrete mixes. Mokarem states that the results of unrestrained shrinkage tests show that the A4 Diabase/Fly ash mixtures exhibited the greatest percent shrinkage, while the A5-Diabase/Slag cement mixtures exhibited the lowest percent shrinkage for the test series. The results of unrestrained shrinkage tests with 95% confidence intervals are shown in Figures 3 and 4.

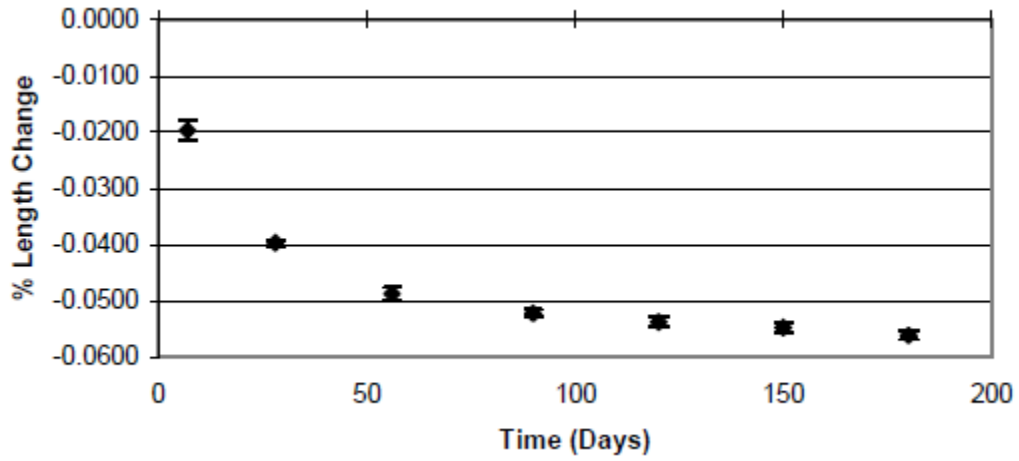

Figure 5: Unrestrained Shrinkage for A4-Diabase/Fly Ash Mixtures (Mokarem, 2002)

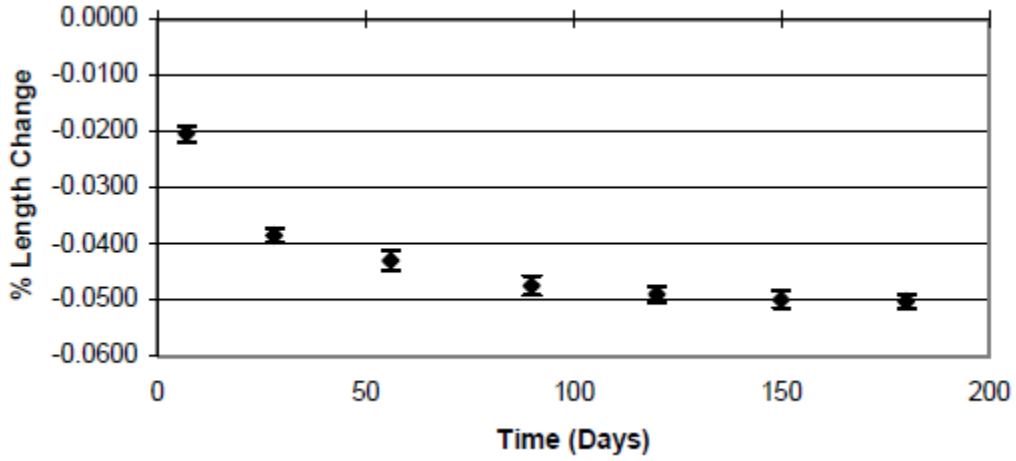

Figure 6: Unrestrained Shrinkage for A4-Diabase/Slag Cement Mixtures (Mokarem, 2002)

The results of the work done at Virginia Tech (increased early strength and reduced shrinkage) appear to be inconsistent with the results found in the literature. More research and test data is needed to make a definitive statement on the effects of adding GGBFS to concrete as a partial replacement for ordinary Portland cement. Given the results of the previous research at Virginia Tech, it was decided to use GGBFS as a 40% (similar to amount used by Mokarem) replacement for Portland cement in order to provide reduction of shrinkage.

2.5 Age Adjusted Effective Modulus Calculation Method

In order to determine the effects of reducing shrinkage and increasing creep on ultimate tensile stresses experienced by a composite girder/deck cross-section, a calculation method must be utilized which can combine the effects of time-dependent creep and shrinkage. The Age-Adjusted Effect Modulus (AAEM) method is able to combine time-dependent effects with external and internal loadings on a composite section in order to determine stresses within a composite cross-section. This method was developed by Trost and further developed by Bazant

(1972). The AAEM method applies an aging factor which modifies the modulus of elasticity of the material, allowing the creep and shrinkage equations to be linearized, leading to a simple set of equations that effectively describe the long-term behavior of the composite system (Wollmann, Anderson et al. 2003). The aging coefficient is given by a complex equation, which for the purposes of concrete loaded between 10 and 100 days can be taken as between 0.7 and 0.9. By using a single, constant aging coefficient, time dependent effect calculations can be simplified and reduced to the solution of a set of linear equations. Figure 7 shows the conditions in a composite girder system which would commonly be used in a precast girder/cast in place topping bridge system.

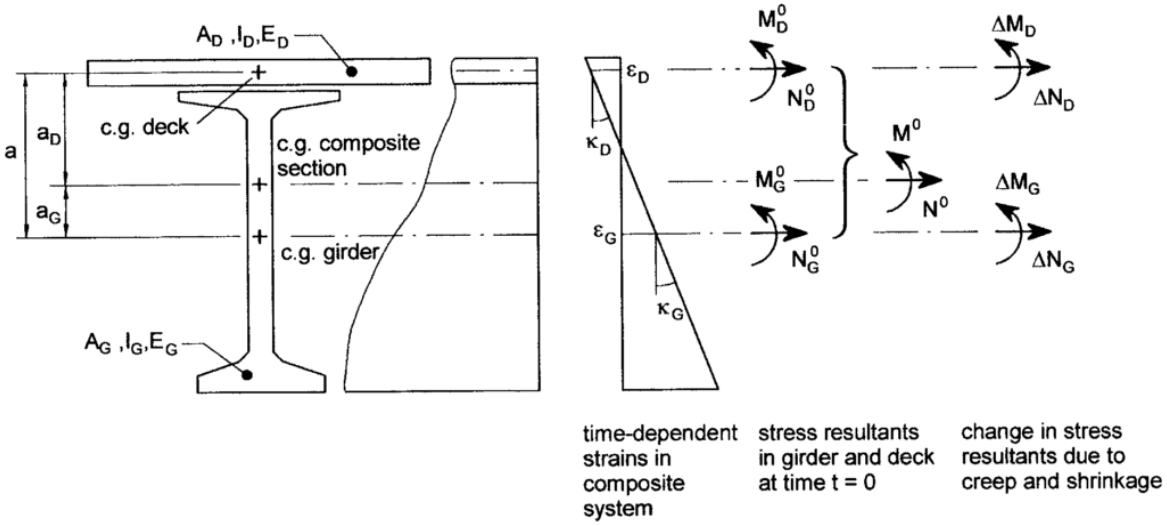

Figure 7 - Strains and forces for composite girder (Wollman et al., 2003)

These forces can be separated into forces and moments which can be used to calculate a system of unknowns via compatibility, equilibrium, and constitutive equations. Further discussion of the AAEM method can be found in the methods section of this thesis. The values for the time-dependent effects (creep and shrinkage) which are obtained via material testing

can be inserted into these equations to determine the ultimate stresses experienced by the cross-section.

In their paper on this subject, Gilbert et al. (2012) discuss the application of the AAEM method toward the determination of time-dependent stresses and deformations in composite floor slabs. Since shrinkage in a concrete cross-section is not linear throughout the depth, the paper also presents the results of laboratory measurements of the non-uniform distribution of shrinkage through the thickness of composite slabs. The authors present the results of extending the AAEM method to calculate the effects of a non-uniform shrinkage gradient by layering the cross-section, with the shrinkage strain specified in each concrete layer depending on its position within the cross-section. Their results showed that the shape of the shrinkage profile through the depth of the slab had a significant effect on the restraint offered by the underlying steel deck and on the magnitude of the time-dependent tensile stresses (caused by shrinkage) near the bottom of the concrete section.

2.6 Creep and Shrinkage Models

A brief summary of each creep and shrinkage model used to compare the results of laboratory material testing on the different concrete mixes contained within this thesis is presented in the methods section. Four models (ACI 209, AASHTO, CEB MC90, and Bazant B3) are used herein to compare the measured creep and shrinkage.

CHAPTER 3: METHODS

This chapter reviews the methods and procedures utilized to generate test data and results.

3.1 Concrete Mix Design

This section encompasses the methods used to design concrete mixes used in the scope of this research project. The base concrete mix used was a 4000 psi topping mix similar to those used by Mokarem (2002) in his research. The proportions used for the mix are shown in Table 1.

Table 1 - A-4 Mix Proportions (Mokarem 2002)

Ingredient	Lbs/yd^3
Cement	635
Fine Aggregate	1286
Coarse Aggregate	1734
Water	286
Total	3941
w/c	0.45

The mix design proportions discussed in the following sections can be seen in Tables 2 and 3. There are three mixes, one including saturated lightweight aggregates (SLWA), one including ground granulated blast furnace slag cement (Slag), and one including both SLWA and Slag (SLWA/Slag). The three normal-weight fly ash mixes are henceforth referred to as NW-FA 1, NW-FA 2, and NW-FA 3.

Table 2 - NW-FA Mix Proportions

Ingredient	NW-FA (All Mixes)
Portland Cement(lb/yd^3)	476
Fly Ash(lb/yd^3)	159
Coarse Aggregate(lb/yd^3)	1780
NW Fine Aggregate (lb/yd^3)	1034
LW Fine Aggregate (lb/yd^3)	0
Water (lb/yd^3)	286
HRWR (ml/yd^3)	2840
Air Entraining Agent (ml/yd^3)	189
W/C Ratio	0.45

Table 3 - Mix Design Proportions

Ingredient	SLWA	Slag	SLWA/Slag
Portland Cement(lb/yd^3)	635	382	382
Slag Cement(lb/yd^3)	0	254	254
Coarse Aggregate(lb/yd^3)	1733	1733	1733
NW Fine Aggregate (lb/yd^3)	666	1285	666
LW Fine Aggregate (lb/yd^3)	403	0	403
Water (lb/yd^3)	261	286	261
HRWR (ml/yd^3)	180	180	180
Air Entraining Agent (ml/yd^3)	180	180	180
W/C Ratio	0.41	0.45	0.41

3.1.1 Saturated Lightweight Aggregate

The amount of saturated lightweight aggregate (SLWA) included in the mix used was determined as per ASTM C1761-12 (Standard Specification for Lightweight Aggregate for Internal Curing of Concrete), specifically X1.3 (Required Amount of Lightweight Aggregate) and X1.4 (Amount of Normal Weight Aggregate to be Replaced). The procedure outlined in ASTM C1761-12 can be seen below.

The amount of lightweight aggregate required for internal curing per unit volume of concrete can be estimated using Equation 1. CS is taken as 0.07 as per ASTM 1761-12 X1.3.3. Mix proportioning is for 1 yd^3 volume of concrete. W/C ratio for SLWA mix was reduced from 0.45 to 0.41 to assist with reduction of drying shrinkage.

Nomenclature

M_{LWA} = mass of (oven dry) lightweight aggregate needed per unit volume of concrete, lb/yd^3
C_f = cementitious materials content for concrete mixture, [lb/yd^3],
CS = chemical shrinkage of cementitious materials at complete (100%) hydration, lb of water/lb of cement
α_{max} = maximum potential degree of hydration of cementitous materials (0 to 1.0)
S = degree of saturation of pre-wetted aggregate relative to the wetted surface-dry condition (0 to 1.0)
W_{LWA} = mass of water released by lightweight aggregate in going from the wetted surface-dry condition to the equilibrium mass at a relative humidity of 94%, expressed as a fraction of the oven-dry mass
OD = relative density (oven-dry) of LWA (lb/ft^3)
$OD_{absorbed}$ = water absorbed to bring oven dry state to SSD (lb/ft^3)
$OD_{released}$ = water available for internal curing (lb/ft^3)

Equations

$$M_{LWA} = \frac{C_F \times CS \times \alpha_{max}}{S \times W_{LWA}} \quad \text{Equation 1}$$

C_f = 635.4

$\propto_{max}$= 1.0

S = 0.07

OD = 65

$OD_{absorbed}$ = 0.12·OD → 7.8 Equation 2

$$OD_{released} = OD_{absorbed} \cdot 0.96 \rightarrow 7.488 \quad \text{Equation 3}$$

$$W_{lwa} = \frac{OD_{released}}{OD} \rightarrow 0.1152 \quad \text{Equation 4}$$

$$M_{1wa} = \frac{C_f.CS\cdot\propto_{max}}{S\cdot W_{1wa}} \rightarrow 402.2 \qquad \text{Equation 5}$$

$$M_{nwa} = M_{1wa} \cdot \frac{100}{65} \rightarrow 618.7 \qquad \text{Equation 6}$$

3.1.2 Slag Mix Design

Slag cement was used to replace Portland cement on a 40% by weight ratio, as per literature review suggestions. Water to cement ratio used was 0.45. This was larger than the 0.41 used for the SLWA mix design since additional water for internal curing was not available from SLWA for the slag mix design. Mix proportions used can be found in Table 2.

3.1.3 Combination of SLWA and Slag Mix Design

SLWA and slag mixes were combined in an attempt to produce a 4 ksi topping mix with the beneficial aspects of both mixes. The water to cement ratio was 0.41 due to the availability of water for internal curing. Mix proportions used can be found in Table 2.

3.2 Material Testing

This section details methods used in testing concrete material specimens for various properties. All concrete specimens were demolded 24 hours after placement and moist cured for 7 days under wet burlap covered by a polyethylene sheet. See Table 4 for a summary of material testing schedules (each mix was tested in identical fashion).

Table 4 - Material Testing Schedule for SLWA, Slag, and SLWA/Slag Mixes

Material Testing at 7, 14, 28, 56, 90 Days	Number of Specimens Fabricated	Creep/Shrinkage Reading Frequency
3 Compressive Str. 3 Splitting Tensile Str. 2 Modulus of Elasticity	30 4x8 Cylinders 5 6x12 Cylinders 2 3x3x11 Prisms 3 Tensile Dogbones	Days 1-7: Daily Days 7-30: Weekly Days 30+: Monthly

3.2.1 Compressive Strength Testing

Compressive strength specimens were fabricated for testing for each concrete mix as per ASTM C192-07 (Standard Practice for Making and Curing Concrete Test Specimens in the Laboratory). Concrete cylinders were used for compressive strength testing at 7, 14, 28, 56, and 90 days of concrete age. All concrete cylinders had dimensions of 4 in. x 8 in. Concrete specimens were tested for compressive strength as per ASTM C39-09a (Standard Test Method for Compressive Strength of Cylindrical Concrete Specimens). Each data point includes the results of three compressive strength tests.

3.2.2 Determination of Modulus of Elasticity

Modulus of elasticity specimens were fabricated for testing for each concrete mix as per ASTM C192-07. Concrete cylinders were used for modulus of elasticity testing at 7, 14, 28, 56, and 90 days of concrete age. All concrete cylinders had dimensions of 4 in. x 8 in. Concrete specimens were tested for modulus of elasticity as per ASTM C469-02 (Standard Test Method for Static Modulus of Elasticity and Poisson's Ratio of Concrete in Compression). Each data point includes the results of two modulus of elasticity tests.

3.2.3 Splitting Tensile Strength Testing

Splitting tensile strength specimens were fabricated for testing for each concrete mix as per ASTM C192-07. Concrete cylinders were used for splitting tensile strength testing at 7, 14, 28, 56, and 90 days of concrete age. All concrete cylinders had dimensions of 4 in. x 8 in. Concrete specimens were tested for splitting tensile strength as per ASTM C496-04 (Standard Test

method for Splitting Tensile Strength of Cylindrical Concrete Specimens). Each data point includes the results of three splitting tensile strength tests.

3.2.4 Unrestrained Shrinkage Testing

Unrestrained shrinkage testing was performed for each concrete mix as per ASTM C157-08 (Standard Test Method for Length Change of Hardened Hydraulic-Cement Mortar and Concrete). This test measures the length change of 3 in. x 3 in. x 11 in. concrete prisms. Specimens were fabricated in steel molds as per ASTM C192-07. Specimens were placed in a controlled environmental room which held temperature (20° C) and humidity (80% RH) constant in an open air environment, allowing them to undergo length change without restraint. Length change measurements were taken as per ASTM C157-08. Readings were taken every 24 hours for 7 days (Starting after 7 days of moist cure), then every 7 days for 30 days, then every 30 days thereafter.

3.2.5 Compressive Creep Testing

Compressive creep testing was performed for each concrete mix as per ASTM C512-02 (Standard Test Method for Creep of Concrete in Compression). Five 6 in. x 12 in. concrete cylinders were fabricated for each mix. Specimens were demolded twenty-four hours after placement and placed under moist cure for seven days. Two sets of DEMEC mechanical strain gauges were installed on each cylinder to determine length change over time. Data from compressive strength testing at seven days was collected and used to calculate the appropriate compressive load for creep testing (40% of seven day compressive strength). Three cylinders were stacked under a hydraulic load cell in a controlled environment and measured to determine a starting point. Cylinders were then loaded to the calculated compressive load and

monitored for length change over time. Readings were taken every 24 hours for 7 days, then weekly for 30 days, then monthly thereafter. The remaining two cylinders were placed adjacent to the creep test and monitored for length change (on-shelf shrinkage). The values obtained from the on-shelf shrinkage testing were subtracted from the creep specimens in order to determine total creep strain. Total creep strain divided by initial elastic strain gives the value of the creep coefficient.

3.2.6 Tensile Creep Testing

Tensile creep testing was performed for each concrete mix, using a test protocol derived from ASTM C512-02. It was desired to use a load application method which did not rely on hydraulics to avoid loss of load over time. A tensile creep frame was developed to apply mechanical tensile loads to concrete specimens utilizing unequally balanced beams supported by a fulcrum. A schematic and photograph of the tensile creep frame are shown in Figure 8 and 9.

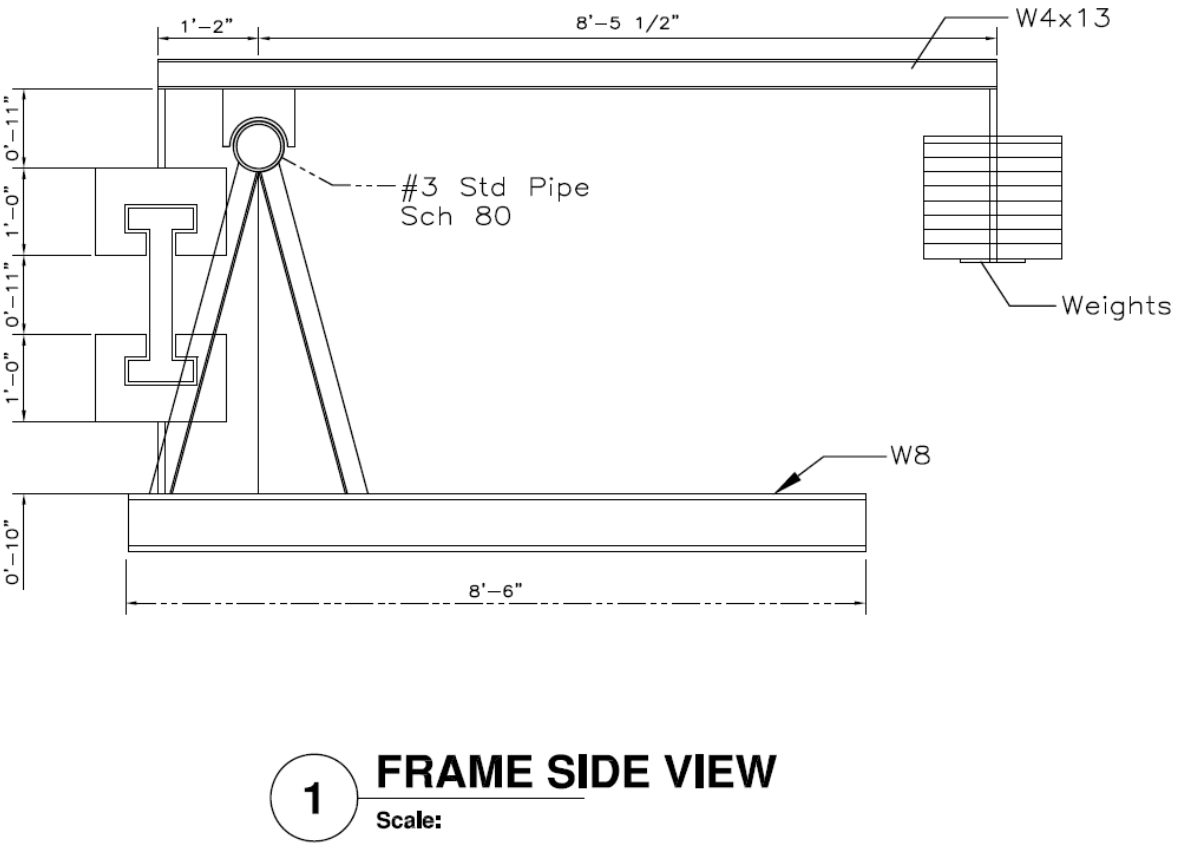

Figure 8- Tensile Creep Frame Schematic Side View

Figure 9- Tensile Creep Frame End View

Concrete specimens were loaded to 40% of seven day tensile capacity as determined by splitting tensile strength tests (after undergoing seven days moist curing). Concrete specimens are 24 in. tall dog bone specimens (see Figures 10 - 12) with 14 in. of 3 in. x 3 in. cross-section. Reinforcement was inserted into the top and bottom area of each specimen to allow load to be transferred to the area of interest without fracturing the specimens. Corners were chamfered to avoid re-entrant corner stress concentrations. Specimens were instrumented with two sets of DEMEC mechanical strain gauges on opposite sides. An 8 in. space between the DEMEC gauges allowed for 3 in. of clear area at either end to allow force to be distributed through the cross section. The specimen was inserted into the grips and held stationary while weights were added at the opposite end of the frame in order to reach the desired loading values. One to two

specimens were loaded on the tensile creep frame as space allowed while one specimen was measured to determine shrinkage values. Shrinkage values were subtracted from creep to determine total tensile creep strain. Note that this experimental procedure neglects the Pickett effect discussed previously, resulting in slightly increased creep values.

Figure 10 - Tensile Creep Specimen

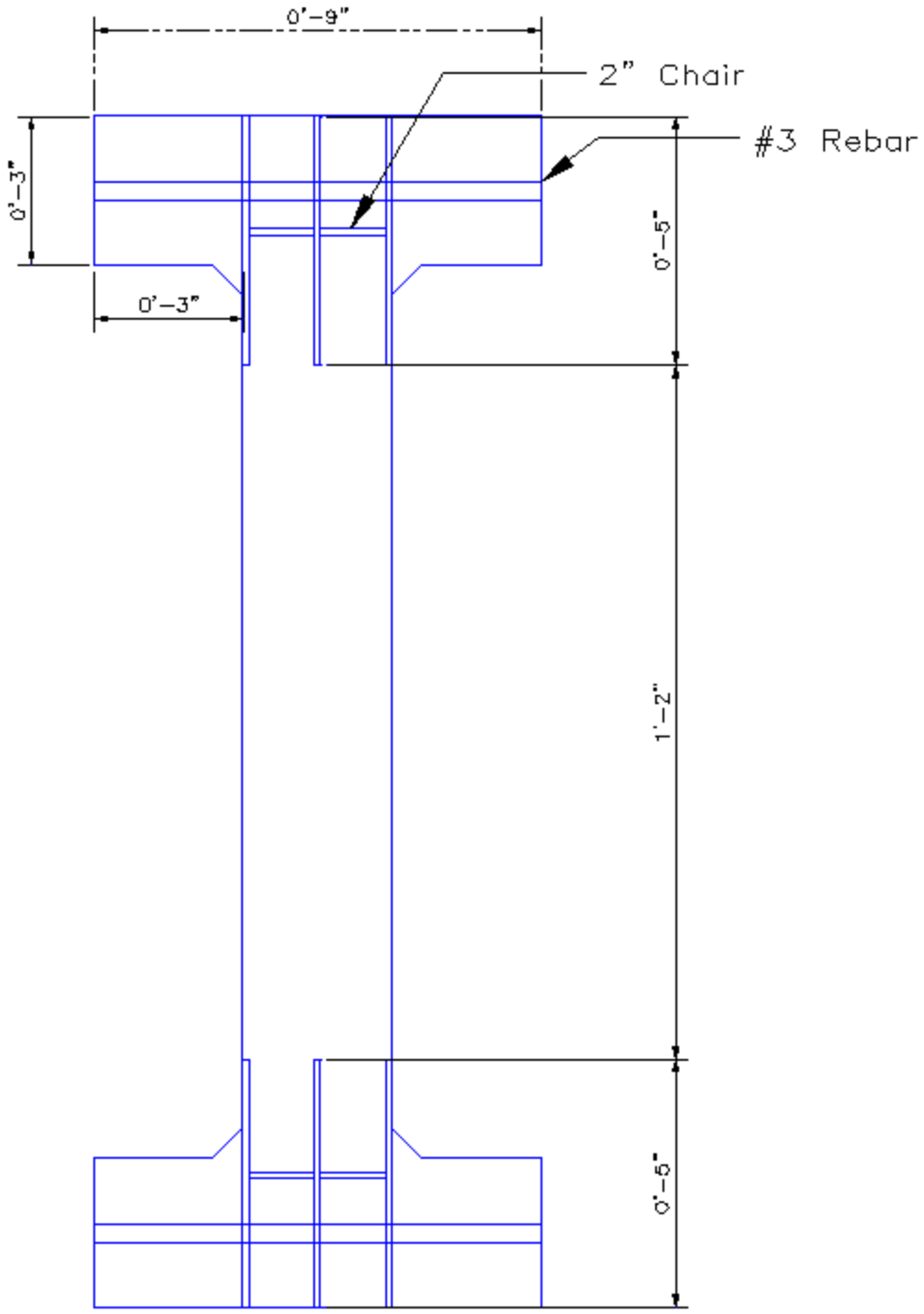

Figure 11 - Tensile Creep Specimen Schematic

Figure 12 - Tensile Creep Specimen Formwork

Grips to hold tensile specimens were fabricated from 8 ksi reinforced concrete, as monetary constraints did not allow for fabrication of steel/aluminum grips. Diagrams of the grips used can be seen in Figures 13 and 14.

Figure 13- Tensile grips with specimen

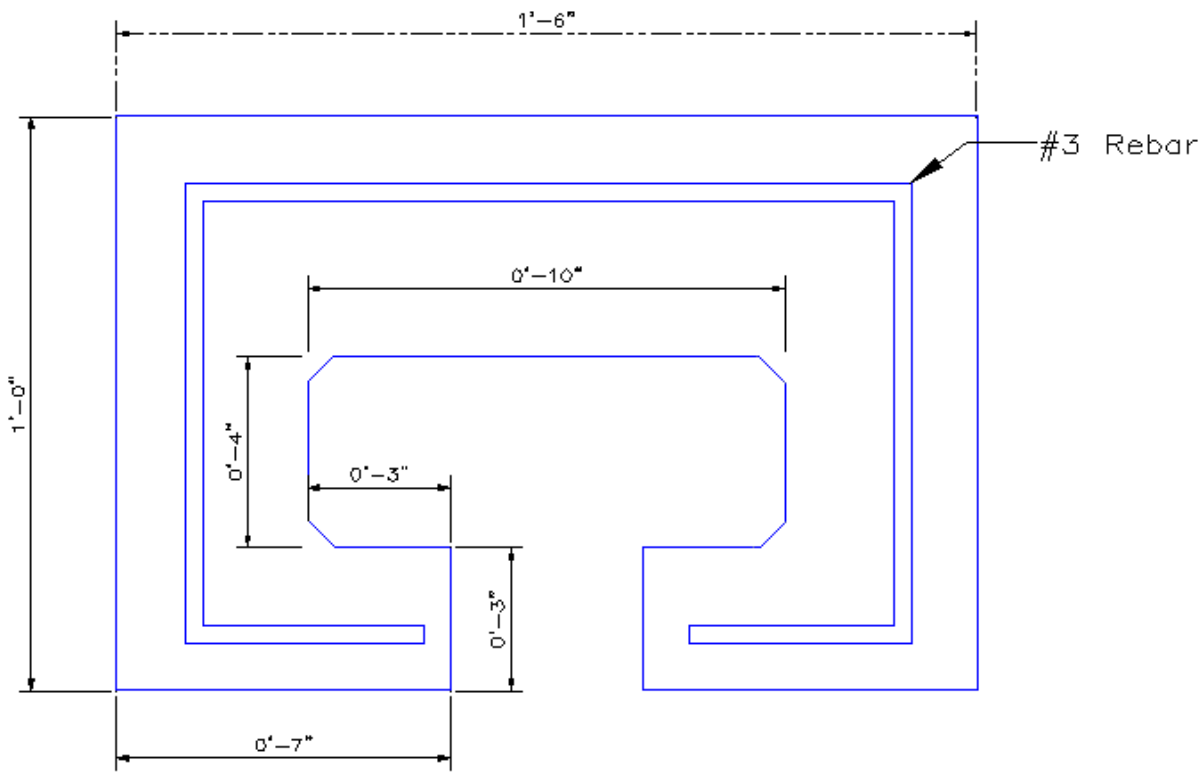

Figure 14 - Tensile Grip Schematic

3.3 Comparisons of Time-Dependent Effects Data to Models

In order to better determine the effects of modifying a 4000 psi concrete mix through the addition of SLWA and slag cement, data from material testing was compared to models. The correlation between data and models is valuable for the purposes of carrying out research in a timely manner by reducing the need for time-consuming and expensive laboratory testing. The data from previous testing was compared against the following creep and shrinkage models: AASHTO, ACI 209, CEB MC90, and Bazant B3(209 2008). As per ACI 209.2R-08 (Guide for Modeling and Calculating Shrinkage and Creep in Hardened Concrete), there are certain assumptions which are applied to the data before it can be analyzed using predictive models.

The main assumptions are explained in the following section. First, shrinkage and creep are additive. Two identical sets of specimens are made and subjected to the same curing and environmental conditions. One set is left unloaded and used to measure shrinkage values, while the other is loaded to 40% of the concrete compressive strength. The shrinkage values from the unloaded specimens are subtracted from the loaded specimens experiencing both shrinkage and creep to determine the values for creep. It is assumed that shrinkage and creep are independent of each other. Second, creep and shrinkage gradients are neglected. It is assumed that shrinkage and creep strains in a specimen occur uniformly through the specimen cross section.

3.3.1 AASHTO Shrinkage and Creep

As per Section 5 of the AASHTO LRFD Bridge Specification, the following equations are used to determine shrinkage strain at a certain age of concrete. The AASHTO model accounts for effects of relative humidity, volume/surface ratio, and compressive strength at time of loading. The time development factor varies with the compressive strength at time of loading.

Nomenclature

ε_{sh} = Shrinkage strain (in./in)
k_s = factor for the effect of the volume to surface ratio of the component
k_{hs} = humidity factor for shrinkage
k_f = factor for the effect of concrete strength
k_{hc} = humidity factor for creep
k_{td} = time development factor
$\Psi(t,t_i)$ = Creep coefficient at concrete age, t and time of initial loading, t_i
$\frac{V}{S}$ = volume to surface ratio
H = relative humidity (%)
f'_{ci} = specified compressive strength of concrete at time of initial loading
t = maturity of concrete (days), defined as age of concrete between time of loading for creep calculations, or end of curing for shrinkage calculations.

AASHTO Equations

Shrinkage Strain:

$$\varepsilon_{sh} = k_s k_{hs} k_f k_{td} * 0.48 \times 10^{-3} \quad \text{Equation 7}$$

$$k_s = 1.45 - 0.13\frac{V}{S} \geq 1.0 \quad \text{Equation 8}$$

$$k_{hs} = 2.00 - 0.014H) \quad \text{Equation 9}$$

$$k_f = \frac{5}{1+ f'_{ci}} \quad \text{Equation 10}$$

$$k_{td} = \frac{t}{61- f'_{ci}+t} \quad \text{Equation 11}$$

Creep Coefficient:

$$\Psi(t,t_i) = 1.9k_s k_{hc} k_f k_{td}\, t_i^{-0.118} \quad \text{Equation 12}$$

$$k_{hc} = 1.56 - 0.008H \quad \text{Equation 13}$$

3.3.2 ACI 209 Shrinkage and Creep

As per ACI 209.2R-08, the following equations are used to determine shrinkage strain at a certain age of concrete. The ACI model also accounts for relative humidity and volume to surface ratio, but not compressive strength. If specifics of mix design are known, factors can be included for aggregate proportions, slump, cement content, and air content.

Nomenclature

$C_c(t)$ = Creep coefficient at time t
t = Time after loading (days)
E_{cmto} = Modulus of elasticity at age of loading
$\varepsilon(t)$ = Total Strain; instantaneous plus creep and shrinkage
$\varepsilon_s(t)$ = Shrinkage strain (in./in.)
$f'_c(t_o)$ = Mean concrete compressive strength at age of loading (psi)
f'_{c28} = Mean 28 day compressive strength (psi)
t_o = Age of concrete loading (days)
γ = Unit weight of concrete (lbs/ft^3)
t_s = Time after the beginning of shrinkage (days)
K_{SS} = Shape and size correction factor for shrinkage
K_{SH} = Relative humidity correction factor for shrinkage
ε_{shu} = Ultimate shrinkage strain (in./in.)
C_{cu} = Ultimate creep coefficient
K_{CH} = Relative humidity correction factor for creep
K_{CA} = Age at loading correction factor
K_{CS} = Shape and size correction factor for creep
H = Relative humidity (%)
V/S = Volume to surface area ratio (in.)
σ = Applied stress (psi)
γ_{sc} = Creep correction factor for slump
γ_{sc} = Shrinkage correction factor for slump
s = Slump (in.)
γ_{ac} = Creep correction factor for fine aggregate percentage

γ_{as} = Shrinkage correction factor for fine aggregate percentage
ψ = Fine aggregate percentage (%)
$\gamma_{\alpha c}$ = Creep correction factor for air content
$\gamma_{\alpha s}$ = Shrinkage correction factor for air content

α = Air content (%)

ACI 209 Equations

Creep Compliance Function

$$\text{Compliance function } (\mu\varepsilon \text{ / psi}) = \frac{1+ C_c(t)}{E_{cmto}} \quad \text{Equation 13}$$

Total Strain

$$\varepsilon(t) = \varepsilon_s(t) + \frac{\sigma}{E_{cmto}} * (1+C_c(t)) \quad \text{Equation 14}$$

Compressive Strength

$$F'_c(t_o) = F'_{c(28)} * \left[\frac{t_o}{b+c*t_o}\right] \quad \text{Equation 15}$$

Table 5 - Compressive Strength Factors for ACI 209

Type of Cement	Moist Cured Concrete	Steam Cured Concrete
I	b = 4.0 c = 0.85	b = 1.0 c = 0.95
II	b = 2.3 c = 0.92	b = 0.7 c = 0.98

Note: Estimate not needed. The experimental $F'_c(t_o)$ was used.

Modulus of Elasticity

$$E_{cmto} = 33(\gamma)^{3/2} * \sqrt{f'_c(t_o)} \quad \text{Equation 16}$$

Note: Estimate not needed. The experimental E_{cmto} was used.

Creep Strain

$$\text{Creep Strain} = \frac{\sigma}{E_{cmto}} * C_c(t) \quad \text{Equation 17}$$

$$C_c(t) = \frac{t^{0.6}}{10+t^{0.6}} * C_{cu} * K_{CH} * K_{CA} * K_{CS} * \gamma_{sc} * \gamma_{ac} * \gamma_{\alpha c} \quad \text{Equation 18}$$

$C_{cu} = 2.35$

$K_{CH} = 1.27 - 0.0067 * H$ Equation 19

$K_{CS} = {}^{2}/_{3} * [1 + 1.13] * e^{(-0.54 * V/S)}$ Equation 20

Table 6 - KCA Factors for ACI 209

Moist Cured Concrete	Steam Cured Concrete
$t, t_o \geq 7$ days, H $\geq 40\%$	$t, t_o \geq 1$ to 3 days, H $\geq 40\%$
$K_{CA} = 1.25\ (t_o)^{-0.118}$	$K_{CA} = 1.13\ (t_o)^{-0.095}$

$\gamma_{sc} = 0.82 + 0.067s$ Equation 21

$\gamma_{ac} = 0.88 + 0.0024\psi$ Equation 22

$\gamma_{\alpha c} = 0.46 + 0.09\alpha$ Equation 23

Shrinkage Strain

$\varepsilon_s(t) = \frac{t_s}{b + t_s} * K_{SS} * K_{SH} * \gamma_{ss} * \gamma_{as} * \gamma_{\alpha s} * \varepsilon_{shu}$ Equation 24

$K_{SS} = 1.2e^{(-0.12 * V/S)}$ Equation 25

$\gamma_{ss} = 0.89 + 0.041s$ Equation 26

For fine aggregate percentage $\leq 50\%$

$\gamma_{as} = 0.30 + 0.014\psi$ Equation 27

For fine aggregate percentage $> 50\%$

$\gamma_{as} = 0.90 + 0.002\psi$ Equation 28

$\gamma_{\alpha s} = 0.95 + 0.008\alpha$ Equation 29

$\varepsilon_{shu} = 780 \times 10^{-6}$ in/in Equation 30

Table 7 - KSH Factors for ACI 209

Humidity	Moist Cured Concrete	Steam Cured Concrete
40 % ≤ H ≤ 80 %	b = 35 t ≥ 7 days	b = 55 t ≥ 1 to 3 days
	K_{SH} = 1.4 – 0.01H	K_{SH} = 1.4 – 0.01H
80 % ≤ H ≤ 100 %	b = 35 t ≥ 7 days	b = 55 t ≥ 1 to 3 days
	K_{SH} = 3 – 0.03H	K_{SH} = 3 – 0.03H

3.3.3 CEB MC90

As per the CEB-FIP Model Code 1990, the following equations are used to determine shrinkage strain at a certain age of concrete. The CEB MC90 model also accounts for relative humidity and strength, cement type, age at loading, and duration of loading.

Nomenclature

$\Phi(t,t_o)$ = Creep coefficient defining creep between time t and t_o
E_c = Modulus of elasticity at 28 days (N/ mm^2)
$E_c(t_o)$ = Modulus of elasticity at age of loading (N/ mm^2)
$\varepsilon(t)$ = Total strain; instantaneous plus creep and shrinkage (mm/mm)
$\varepsilon_{cs}(t-t_s)$ = Shrinkage strain between time t and t_s (mm/mm)
t = Age of concrete after casting (days)
t_s = Age of concrete at the beginning of shrinkage (days)
f_{cm} = Mean 28 day concrete compressive strength (N/mm^2)
f_{ck} = Characteristic compressive strength with 95% confidence (N/mm^2)
t_o = Age of concrete at loading (days)
Φ_o = Notional creep coefficient
$\beta_c(t-t_o)$ = Coefficient describing creep development with time after loading
Φ_{RH} = Factor to allow for relative humidity on the notional creep coefficient (Φ_o)
$\beta(f_{cm})$ = Factor to allow for effect of concrete strength on the notional creep coefficient (Φ_o)
$\beta(t_o)$ = Factor to allow for the effect of age of concrete at loading on the notional creep coefficient (Φ_o)
RH = Relative humidity (%)
A_c = Cross-section area of member (mm^2)
u = Perimeter of member in contact with the atmosphere (mm)
$h_o = 2A_c/u$ = Notional size of member (mm)
β_H = Coefficient to allow for the effect of relative humidity and the notional member

size (h_o) on creep
ε_{cso} = Notional shrinkage coefficient
$\beta_s(t-t_s)$ = Equation describing development of shrinkage with time
$\varepsilon_s(f_{cm})$ = Factor to allow for the effect of concrete strength on shrinkage
β_{RH} = Coefficient to allow for the effect of relative humidity on the notional shrinkage coefficient (ε_{cso})
β_{sc} = Coefficient depending on type of cement
β_s = Coefficient to describe the development of shrinkage with time
σ = Applied stress (N/ mm^2)
α = Coefficient for cement type
$t_{o,T}$ = temperature adjusted age of concrete at loading (days)
Δt_i = number of days at temperature T
$T(\Delta t_i)$ = temperature during time period Δt_i (^{o}C)
n = number of time intervals considered

CEB 90 Model Code Equations

Total Strain

$$\varepsilon(t) = \varepsilon_{cs}\,(t - t_s) + \left[\frac{\Phi(t,t_o)}{\mathrm{E_c}} + \frac{1}{E_c(t_o)}\right]\sigma \qquad \text{Equation 31}$$

Mean Concrete Strength

$$f_{cm} = f_{ck} + 8\ \mathrm{N/mm2} \qquad \text{Equation 32}$$

Note: Estimate not needed. The experimental f'$_{c28}$ was used.

Modulus of Elasticity at Age t

$$E_c = 10000\ \sqrt[3]{f_{cm}} \qquad \text{Equation 33}$$

$$E_c(t_0) = (E_c)\ e^{\left[\frac{S}{2}\left(1-\sqrt{\frac{28}{t}}\right)\right]} \qquad \text{Equation 34}$$

S = 0.38, slow hardening cement
0.25, normal and rapid hardening cement
0.20, rapid hardening high strength

Note: Estimate not needed. The experimental E_c and $E_c t_o$ was used.

Creep Compliance Function

$$\text{Compliance function } [\mu\varepsilon/\text{ psi}] = \left[\frac{\Phi(t,to)}{E_c} + \frac{1}{E_c(t_o)}\right] \quad \text{Equation 35}$$

$$\Phi(t, t_o) = (\Phi_o) * \beta_c(t - t_o) \quad \text{Equation 36}$$

$$\Phi_o = \Phi_{RH} * \beta(f_{cm}) * \beta(t_o) \quad \text{Equation 37}$$

$$\Phi_{RH} = 1 + \frac{(1 - \frac{RH}{100})}{0.1 * \sqrt[3]{h_o}} \quad \text{Equation 38}$$

$$\beta(f_{cm}) = \frac{16.8}{\sqrt{f_{cm}}} \quad \text{Equation 39}$$

$$\beta(t_o) = \frac{1}{(0.1 + t_0^{0.2})} \quad \text{Equation 40}$$

$$\beta_c(t - t_o) = \frac{(t - t_o)^3}{[\beta_H + (t - t_o)]^{0.3}} \quad \text{Equation 41}$$

$$\beta_H = 1.5 * [1 + (0.012 * RH)^{18}] (h_o) + 250 \leq 1500 \text{ days} \quad \text{Equation 42}$$

The effect of cement type can be modified for the creep coefficient by modifying the age at loading:

$$t_o = t_{o,T} * \left[\frac{9}{2 + (t_{o,T})^{1.2}} + 1\right]^{\alpha} \geq 0.5 \text{ days} \quad \text{Equation 43}$$

$$\boldsymbol{t_{o,T}} = \sum_{i=1}^{n} \boldsymbol{\Delta} t_i * e^{-\left[\frac{4000}{273 + T\{\Delta_i\}} - 13.65\right]} \quad \text{Equation 44}$$

Table 8 - α Factors for CEB MC90

Cement Type	A
SL	-1
N, R	0
RS	1

Shrinkage Strain

$$\varepsilon_{cs}(t - t_s) = (\varepsilon_{cso}) * \beta_s(t - t_s) \quad \text{Equation 45}$$

$$\varepsilon_{cso} = \varepsilon_s(f_{cm}) * (\beta_{RH}) \quad \text{Equation 46}$$

$$\varepsilon_s(f_{cm}) = [160 + \beta_{SC}(90 - f_{cm})] * 10^{-6} \quad \text{Equation 47}$$

Table 9 - βSC Factors for CEB MC90

Type of Cement	$\boldsymbol{\beta_{SC}}$
Slow hardening (SL)	4
Normal and rapid hardening (N, R)	5
Rapid hardening high strength (RS)	8

Table 10 - βRH Factors for CEB MC90

Humidity	$\boldsymbol{\beta_{RH}}$
40 % ≤ RH ≤ 99 %, stored in air	-1.55 x β_{sRH}
RH ≥ 99 %, immersed in water	0.25

$$\beta_{RH} = 1 - \left(\frac{RH}{100}\right)^3 \quad \text{Equation 48}$$

$$\boldsymbol{\beta_s}(t - t_s) = \sqrt{\frac{(t-t_s)}{[0.035*h_0^2 + (t-t_s)]}}$$ Equation 49

3.3.4 Bazant B3

As per Bazant's B3 model, the following equations are used to determine shrinkage and creep strains at a certain age of concrete. Bazant's model is highly complex and has been designed to be able to account for any type of deviation from a standard concrete mix.

Nomenclature

$J(t,t')$ = Creep compliance function; creep plus elastic (always $x10^{-6}$/psi)
α = Thermal expansion coefficient
$\Delta T(t)$ = Temperature change from reference at time t
$C_o(t,t')$ = Compliance function for basic creep
$C_d(t,t',t_o)$ = Compliance function for additional creep due to drying
$\varepsilon(t)$ = Total Strain; instantaneous plus creep and drying (in/in)
$\varepsilon_{sh}(t)$ = Shrinkage Strain (in./in.)
f'_c = Mean 28 day concrete compressive strength (psi)
f_{ck} = Specified concrete compressive strength at 28 days (psi)
E_{28} = Modulus of elasticity at 28 days (psi)
q1 = Instantaneous strain due to unit stress
q2 = Aging visco-elastic compliance
q3 = Non-aging visco-elastic compliance
q4 = Flow compliance
q5 = Creep at drying
t = Age of concrete after casting (days)
t' = Age of concrete at loading (days)
t_o = Age of concrete at the beginning of shrinkage (days)
c = Cement content of concrete (lbs/ft^3)
w/c = Water to cement ratio by weight
a/c = Aggregate to cement ratio by weight
H(t) = Spatial average of pore relative humidity within cross section
S(t) = Time function for shrinkage
$\varepsilon_{sh\infty}$ = Ultimate shrinkage strain (negative, always x 10^{-6} in./in.)
w = Water content of concrete (lbs/ft^3)
h = Relative humidity (decimal)
τ_{sh} = Shrinkage half-time (days)
k_s = Cross section shape factor
V/S = Volume to surface are ratio (in.)

$D = 2(V/S)$ = Effective cross-section thickness (in.) Equation 50
k_h = Humidity function for shrinkage

B3 Model Equations

Creep Compliance Function

$$J(t,t') \ [\mu\varepsilon/\ psi] = q_1 + C_o(t,t') + C_d(t,t',t_o)$$ Equation 51

Total Strain

$$\varepsilon(t) = J(t,t')\sigma + \varepsilon_{sh}(t) + \alpha\Delta T$$ Equation 52

Note: Assume specimens are in thermal equilibrium with room at time of loading.

Mean Compressive Strength

$$f'_c = f_{ck} + 1200$$ Equation 53

Note: Estimate not needed. The experimental f'_c was used.

Elastic Strain and Modulus of Elasticity

$$q_1 = \frac{0.6 * 10^6}{E_{28}}$$ Equation 54

$$E_{28} = 57000\ (f_c')^{1/2}$$ Equation 55

Note: Estimate not needed. The experimental E_{28} was used

Basic Creep Compliance

$$C_o(t,t') = q_2 * Q(t,t') + q_3 * \ln(1 + (t - t')^n) + q_4 * \ln(t / t')$$ Equation 56

$$Q(t,t') = Q_f(t') * \left[1 + \frac{[Q_f(t')]^{r\{t'\}}}{[Z(t,t')]^{r\{t'\}}}\right]^{\frac{-1}{r\{t'\}}}$$ Equation 57

$$Q_f(t') = [0.086 * (t')^{2/9} + 1.21 * (t')^{4/9}]^{-1}$$ Equation 58

$$Z(t, t') = (t')^{-m} * \ln(1+ (t - t')^{n})$$ Equation 59

$$m = 0.5$$

$$n = 0.1$$

$$r(t') = 1.7 * (t')^{0.12}+8$$ Equation 60

$$q_2 = 451.1 * (c)^{0.5} * (f_c')^{-0.9}$$ Equation 61

$$q_3 = 0.29 * (w/c)^{4} * q_2$$ Equation 62

$$q_4 = 0.14 * (a/c)^{-0.7}$$ Equation 63

Drying Creep Compliance

$$C_d(t,t',t_o) = q_5[\exp\{-8 * H(t)\} - \exp\{-8 * H(t')\}]^{1/2}$$ Equation 64

$$H(t) = 1 - (1-h) * S(t)$$ Equation 65

$$H(t') = 1- (1-h) * S(t')$$ Equation 66

$$q_5 = 7.57 \text{ x } 10^5 * (f'_c)^{-1} * (\varepsilon_{sh\infty})^{-0.6}$$ Equation 67

$$S(t) = \tanh\sqrt{\frac{t-t_0}{\tau_{sh}}}$$ Equation 68

$$S(t') = \tanh\sqrt{\frac{t'-t_0}{\tau_{sh}}}$$ Equation 69

$$\tau_{sh} = k_t(k_s * D)^2$$ Equation 70

$$k_t = 190.8(t_0)^{-0.08}(f_c')^{-0.25}$$ Equation 71

Table 11 - Ks Factors for Bazant B3

Type of Member or Structure	K_s
Infinite slab	1
Infinite cylinder	1.15
Infinite square prism	1.25
Sphere	1.3
Cube	1.55
undefined member	1

Shrinkage Strain

$$\varepsilon_{sh\infty}(t,t_0) = -\varepsilon_{sh\infty} * k_h * S(t)$$ Equation 72

$$\varepsilon_{sh\infty} = \alpha_1\alpha_2(26(w)^{2.1}(f_c')^{-0.28} + 270) \times 10^{-6}$$ Equation 73

$$S(t) = \tanh\sqrt{\frac{t-t_0}{\tau_{sh}}}$$ Equation 74

Table 12 - α1 Factors for Bazant B3

Type of Cement	α_1
I	1
II	0.85
III	1.1

Table 13 – α2 Factors for Bazant B3

Type of Curing	α_2
Steam cured	0.75
Water Cured or h = 100%	1
Sealed during curing	1.2

3.4 Age Adjusted Effective Modulus Parametric Study

In order to determine the effects of increasing creep and decreasing shrinkage, the AAEM method was used to determine total stresses throughout the depth of the concrete cross-section. The cross section used was the tapered Inverted-Tee section tested at Virginia Tech during the summer of 2012. Further information on the Inverted-Tee testing can be found in Mercer (Mercer 2012). The AAEM method was applied to the tapered cross section (shown in Figure 15) with a cast in place topping depth of 7 in. and precast girder depth of 18 in. The procedure used to apply the AAEM method to the cross section can be seen below.

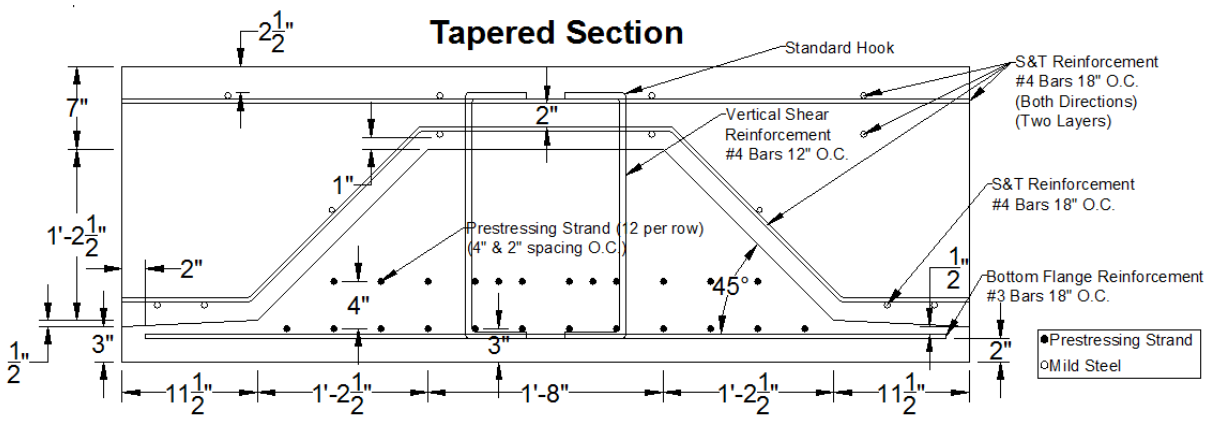

Figure 15- Inverted Tee Tapered Section

3.4.1 AAEM Method

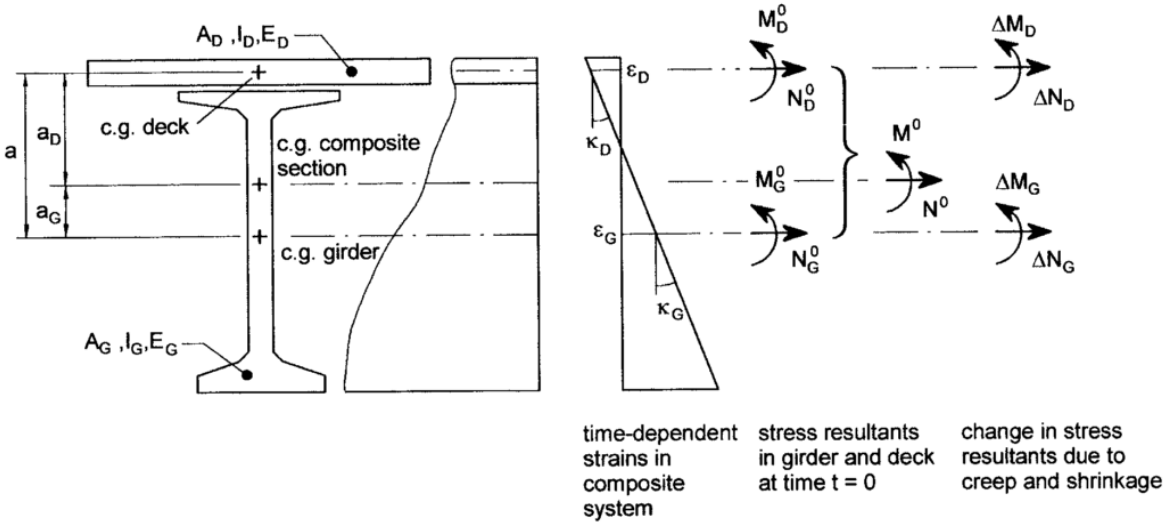

Figure 16 - Strains and forces for composite girder (Wollman et al., 2003)

The procedure for using the AAEM method is displayed below. See Fig. 16 for clarification on location and types of loading.

Nomenclature

n = Modular ratio of deck concrete to girder concrete
E_D, E_G = Modulus of elasticity for deck and girder, respectively
A_D, A_G = Area of deck and girder, respectively
A_c = Area of transformed composite section
a = Distance between centroid of deck and centroid of girder
a_D = Distance between centroid of deck and centroid of composite section
a_G = Distance between centroid of girder and centroid of composite section
S_c = First area moment of the transformed deck section about the centroid of the composite section
I_D, I_G = Moment of inertia of deck and girder, respectively, about their own centroids
I_C = Moment of inertia of the composite section about its own centroid.
ε_D, ε_G = Strain in the deck and girder, respectively
κ_D, κ_G = Curvature of deck and girder, respectively
N_D^0, N_G^0 = Initial normal force on deck and girder, respectively
M_D^0, M_G^0 = Initial moment on deck and girder, respectively
M^0, N^0 = Initial normal force and moment on composite section, respectively
ΔN_D, ΔN_G = Change in normal force on deck and girder, respectively
ΔM_D, ΔM_G = Change in moment on deck and girder, respectively
φ_D, φ_G = Creep coefficient for deck and girder, respectively
ε_{sD}, ε_{sG} = Shrinkage strain for deck and girder, respectively
μ = Aging Coefficient

Composite Section Properties

$$n = \frac{E_D}{E_G}$$ Equation 75

$$A_c = A_G + nA_D$$ Equation 76

$$a_d = \frac{A_G}{A_C} a$$ Equation 77

$$a_G = \frac{nA_D}{A_C} a$$ Equation 78

$$S_c = nA_D a_D$$ Equation 79

$$I_c = I_G + nI_D + aS_c$$ Equation 80

Component Forces

$$N_D = \frac{nA_D}{A_C} N - M \frac{S_C}{I_C}$$ Equation 81

$$N_G = \frac{A_G}{A_C} N - M \frac{S_C}{I_C}$$ Equation 82

$$M_D = \frac{nI_D}{I_C}$$ Equation 83

$$M_G = \frac{I_G}{I_C}$$ Equation 84

Compatibility Requirements

$$\kappa_D = \kappa_G = \kappa$$ Equation 85

$$\varepsilon_D = \varepsilon_G + \kappa * \mathbf{a}$$ Equation 86

Equilibrium Requirements

$$\Delta N_D + \Delta N_G = 0$$ Equation 87

$$\Delta M_D + \Delta M_G + \Delta N_G * a = 0$$ Equation 88

Constitutive Equations

$$\varepsilon_D = \frac{N_D^0}{E_D A_D} \varphi_D + \frac{\Delta N_D}{E_D A_D} (1 + \mu \varphi_D) + \varepsilon_{sD}$$ Equation 89

$$\varepsilon_G = \frac{N_G^0}{E_G A_G} \varphi_G + \frac{\Delta N_G}{E_G A_G} (1 + \mu \varphi_G) + \varepsilon_{sG}$$ Equation 90

$$\kappa_D = \frac{M_D^0}{E_D I_D} \varphi_D + \frac{\Delta M_D}{E_D I_D} (1 + \mu \varphi_D)$$ Equation 91

$$\kappa_G = \frac{M_G^0}{E_G I_G} \varphi_G + \frac{\Delta M_G}{E_G I_G} (1 + \mu \varphi_G)$$ Equation 92

Given these eight equations and eight unknowns (ΔM_D, ΔM_G, ΔN_D, ΔN_G, κ_D, κ_G, ε_D, and ε_G), a system of equations can be formulated. The system of equations is then solved using a computer program.

The values for ultimate creep and shrinkage can be modified in order to determine the stress distribution resulting from differential shrinkage. The results of varying creep and shrinkage can be found in the results section of this thesis (Results of AAEM Parametric Study).

CHAPTER 4: RESULTS

4.1 Introduction

This chapter presents the results of the testing performed on various concrete mixes, including compressive strength, modulus of elasticity, restrained shrinkage, unrestrained shrinkage, compressive creep, and tensile creep. Also presented are the results of a parametric study of concrete mixes designed to have more creep and less shrinkage over time, as well as comparisons between testing results and time-dependent effect models. These test results encompass three normal-weight concrete topping mixtures containing fly ash which are compared to the three mixtures incorporating SLWA, slag cement, and a combination of the two. Test procedures are given in Chapter 3.

4.2 Compressive Strength

Tables 14 to 16 along with Figure 17 present the results of compressive strength testing on three normal-weight fly ash mixtures (henceforth referred to as NW-FA 1, NW-FA 2, and NW-FA 3).

Table 14 - Compressive Strength of NW-FA 1

Age (days)	Compressive Strength of 4x8 Cylinders, 4 ksi 1/31/2012 Mix Date (NW-FA 1)			
	Failure Load (lb)	Compressive Strength (psi)	Failure Mode	Avg. Strength (psi)
7	34500	2750	Shear	3110
7	42750	3400	Cone/Shear	
7	40000	3180	Cone	
14	42500	3380	Cone	3340
14	42000	3340	Cone	
14	41500	3300	Cone	
28	49500	3940	Cone/Shear	3810
28	47750	3800	Shear	
28	46500	3700	Shear	

Table 15 - Compressive Strength of NW-FA 2

Age (days)	Compressive Strength of 4x8 Cylinders, 4 ksi 2/7/2012 Mix Date (NW-FA 2)			
	Failure Load (lb)	Compressive Strength (psi)	Failure Mode	Avg. Strength (psi)
7	32000	2550	Shear	2610
7	33500	2670	Cone/Shear	
7	33000	2630	Cone	
14	42500	3380	Cone	3340
14	42000	3340	Cone	
14	41500	3300	Cone	
24	42000	3340	Shear	3390
24	42500	3380	Shear	
28	43500	3460	Cone	3380
28	41500	3300	Shear	
28	42500	3380	Shear	

Table 16 - Compressive Strength of NW-FA 3

Age (days)	Compressive Strength of 4x8 Cylinders, 4 ksi 6/27/2012 Mix Date (NW-FA 3)			
	Failure Load(lb)	Compressive Strength (psi)	Failure Mode	Avg. Strength psi)
7	45250	3600	Shear	3500
7	43750	3480	Shear	
7	43000	3420	Shear	
14	53000	4220	Shear	4090
14	50000	3980	Shear	
14	51250	4080	Shear	
28	48500	3860	Cone/Shear	3990
28	52500	4180	Cone/Shear	
28	49500	3940	Cone/Shear	
56	38250	3040	Defective	3980
56	52000	4140	Shear	
56	48000	3820	Shear	

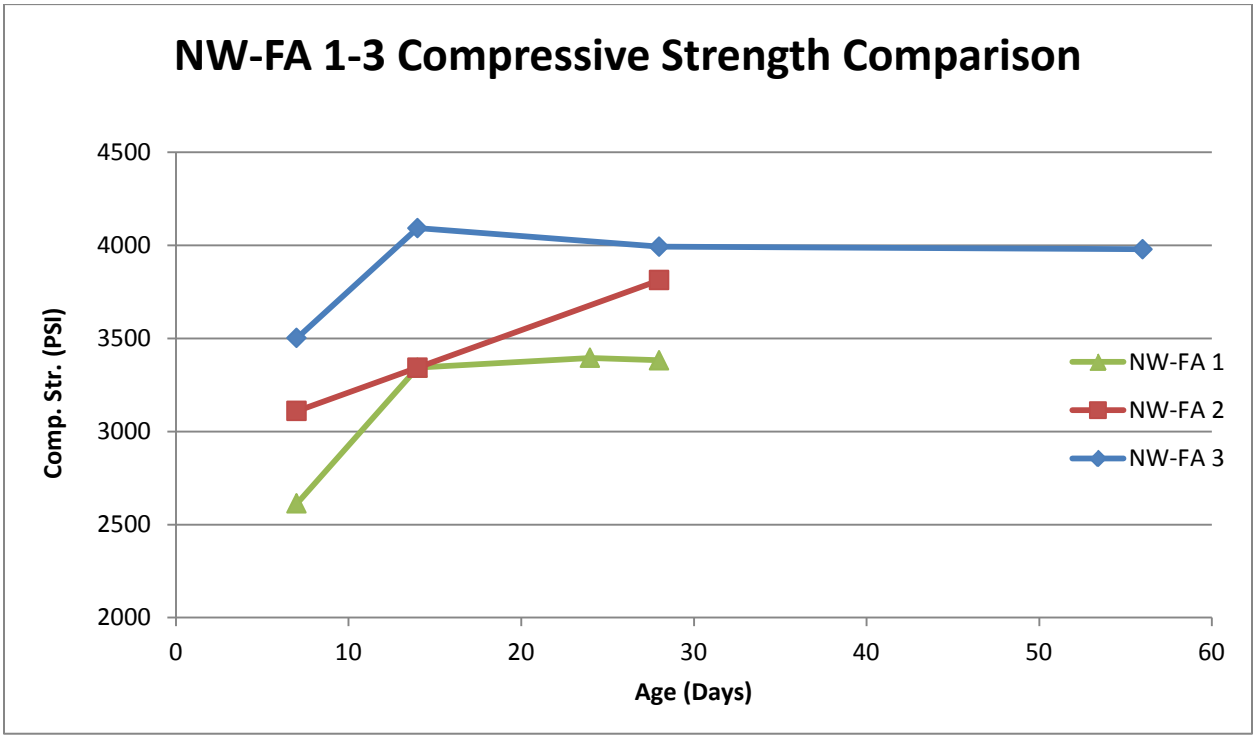

Figure 17 - Comparison of Compressive Strength Values of NW-FA 1-3

Tables 17-19 along with Figure 18 show the results of compressive strength testing on three additional bridge deck topping mixes (henceforth referred to as SLWA, Slag, and SLWA/Slag).

Table 17 - Compressive Strength of SLWA

Age (days)	Compressive Strength of 4x8 Cylinders, SLWA 5/20/2013 Mix Date			
	Failure Load (lb)	Compressive Strength (psi)	Failure Mode	Avg. Strength (psi)
7	36500	2910	Shear	2650
7	30000	2390	Shear	
7	33250	2650	Shear	
14	48000	3820	Cone/Shear	3280
14	38250	3040	Cone/Shear	
14	37500	2980	Cone/Shear	
28	49250	3920	Shear	3540
28	41500	3300	Cone	
28	42500	3380	Cone	
56	50250	4000	Shear	3610
56	43250	3440	Cone	
56	42500	3380	Shear	

Table 18 - Compressive Strength of Slag

Age (days)	Compressive Strength of 4x8 Cylinders, SLAG 6/12/2013 Mix Date			
	Failure Load (lb)	Compressive Strength (psi)	Failure Mode	Avg. Strength (psi)
7	52000	4140	Shear	4080
7	51750	4120	Shear	
7	50000	3980	Shear	
14	63000	5010	Shear	4830
14	60750	4830	Shear	
14	58500	4660	Shear	
28	67500	5370	Cone/Shear	5370
28	67500	5370	Cone/Shear	
28	67500	5370	Cone/Shear	
56	68000	5410	Shear	5410
56	71000	5650	Shear	
56	65000	5170	Shear	

Table 19 - Compressive Strength of SLWA/Slag

Age (days)	Compressive Strength of 4x8 Cylinders, SLWA/SLAG 7/20/2013 Mix Date			
	Failure Load (lb)	Compressive Strength (psi)	Failure Mode	Avg. Strength (psi)
7	34500	2750	Shear	3660
7	53000	4220	Shear/Cone	
7	50500	4020	Shear	
14	43000	3420	Cone	4130
14	54500	4340	Cone	
14	58000	4620	Shear/Cone	
28	43000	3420	Shear	4560
28	65000	5170	Cone/Shear	
28	64000	5090	Shear	

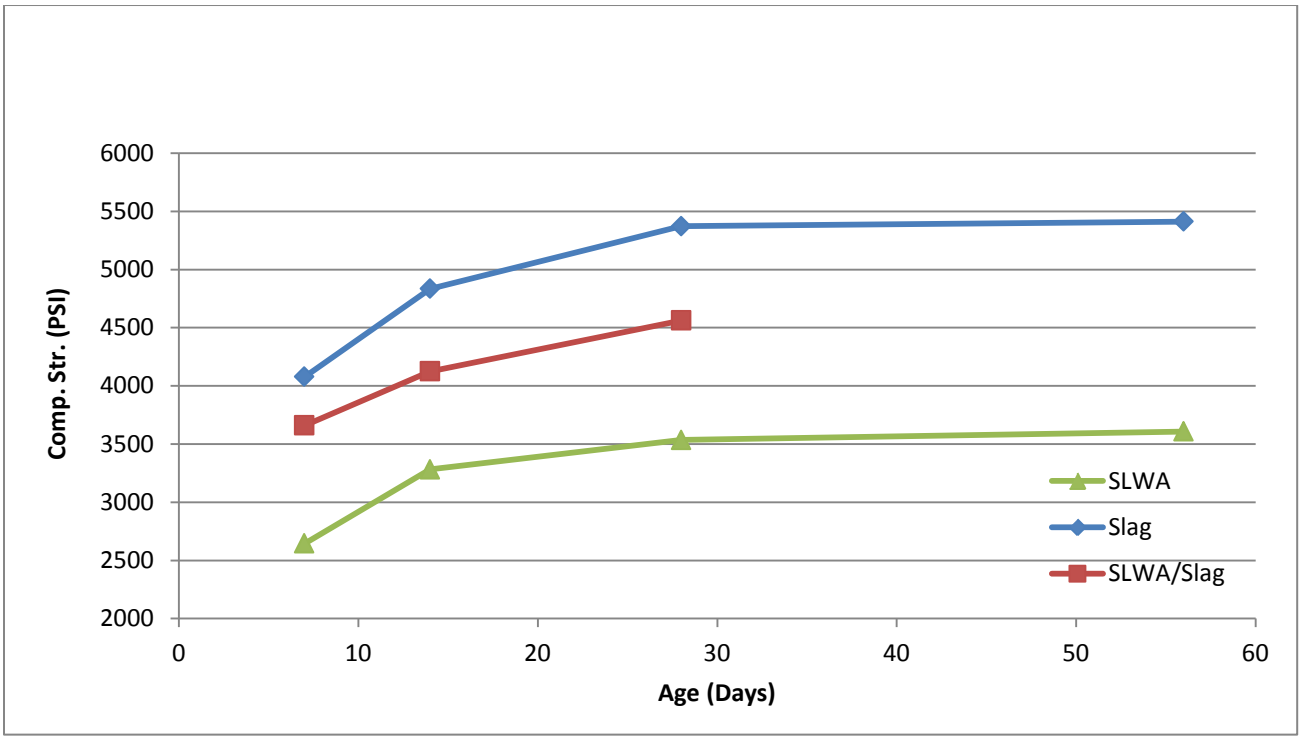

Figure 18 - SLWA Slag SLWA/Slag Compressive Str. Comparison

4.3 Unrestrained Shrinkage

Figures 19-21 present the results of unrestrained shrinkage testing on three normal-weight fly ash mixtures. Note that Series 2 in Figure 19 was considered an outlier and was not utilized when calculating results.

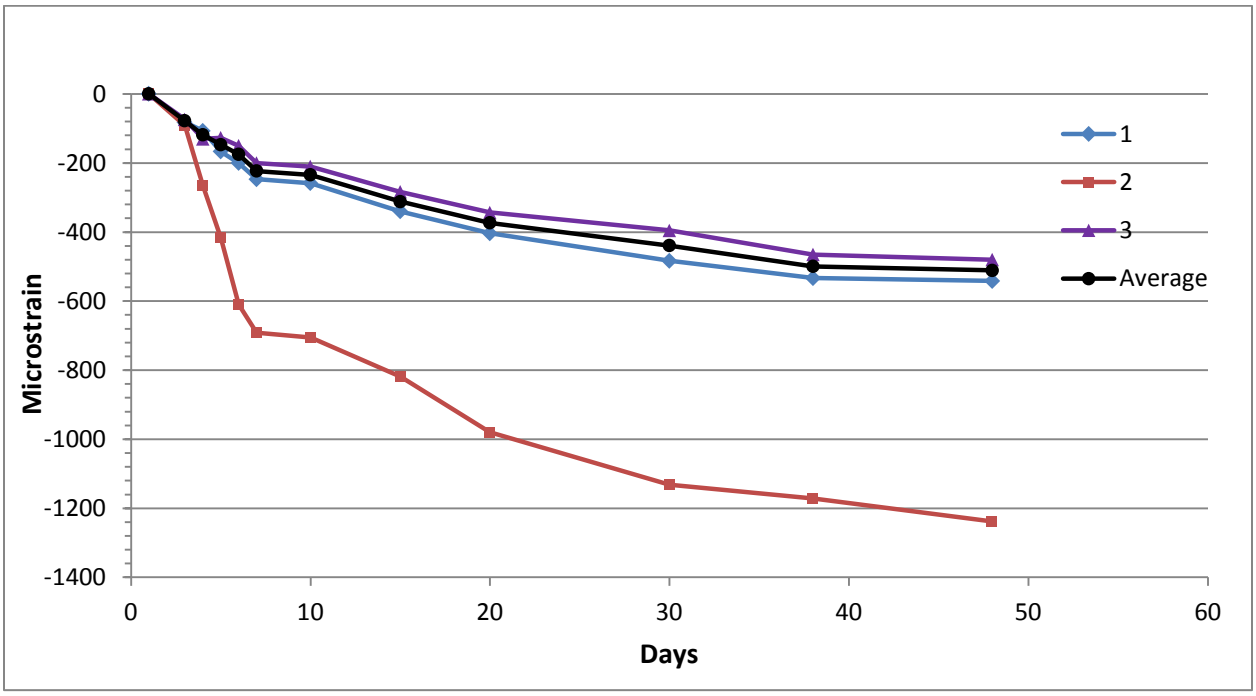

Figure 19 - Unrestrained Shrinkage for NW-FA 1

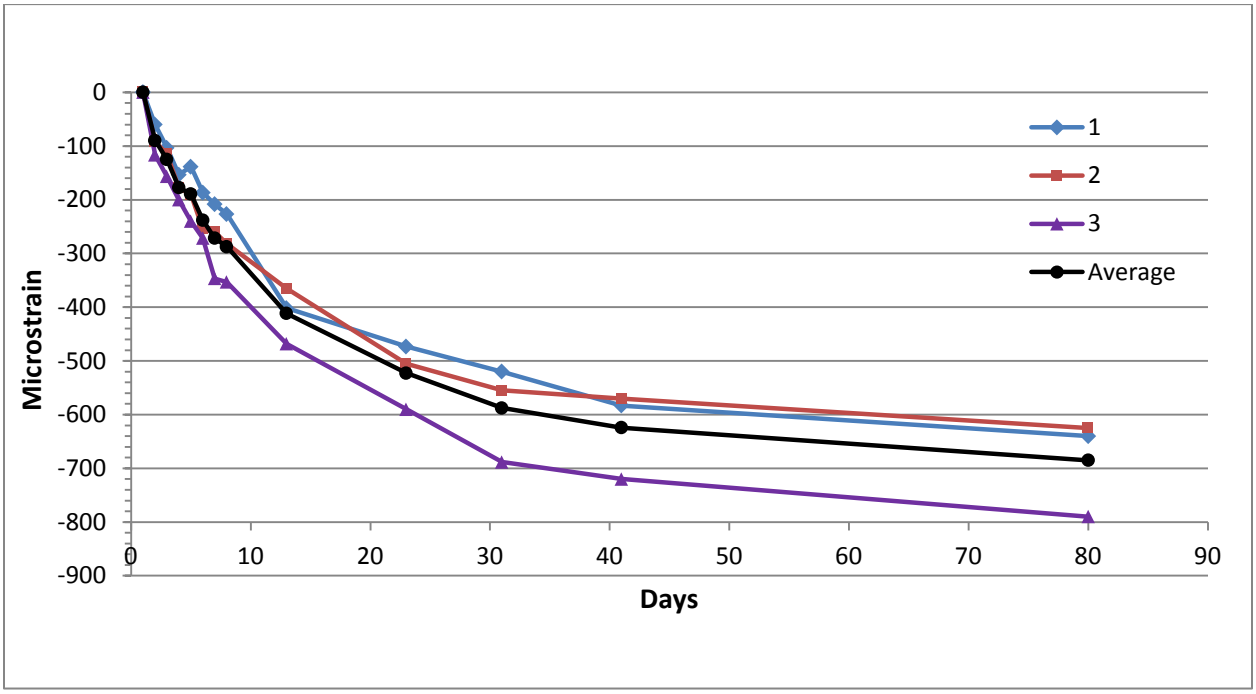

Figure 20 - Unrestrained Shrinkage for NW-FA 2

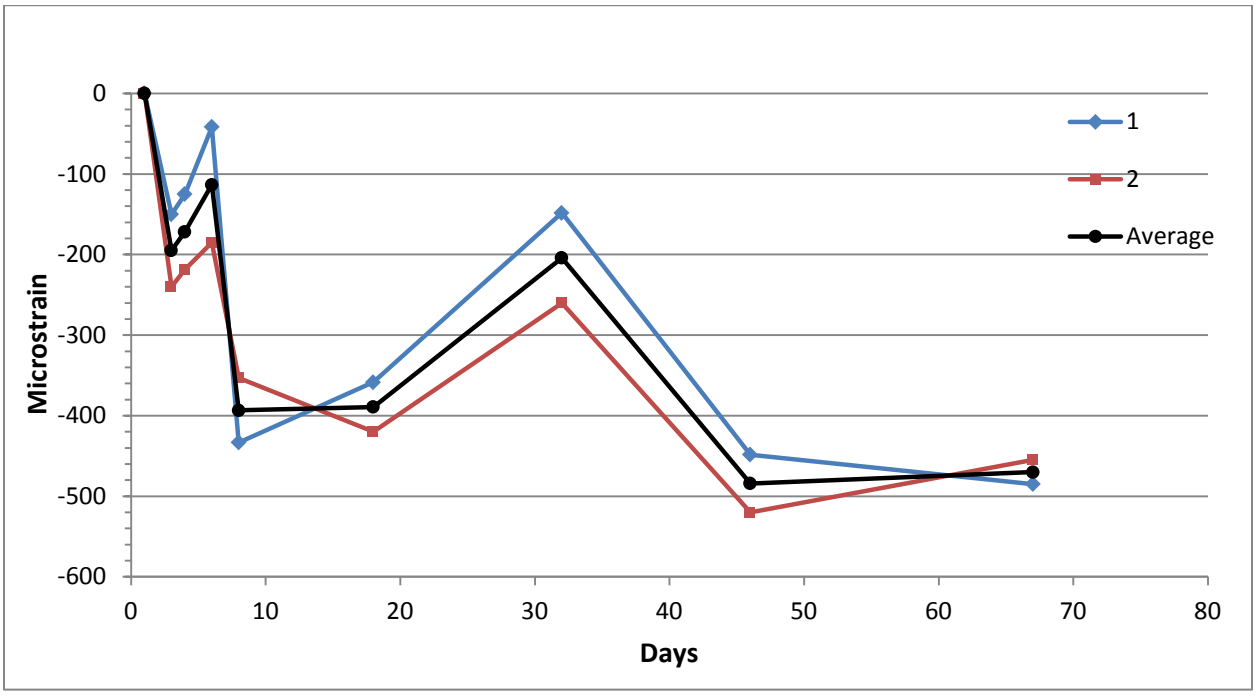

Figure 21 - Unrestrained Shrinkage Strain for NW-FA 3

The fluctuations in the shrinkage strain in NW-FA 3 are due to mechanical failure of the environmental chamber, causing sudden increases in temperature and humidity, leading to swelling of the shrinkage specimens.

Figures 22-24 present the results of unrestrained shrinkage testing on three additional bridge deck topping mixtures.

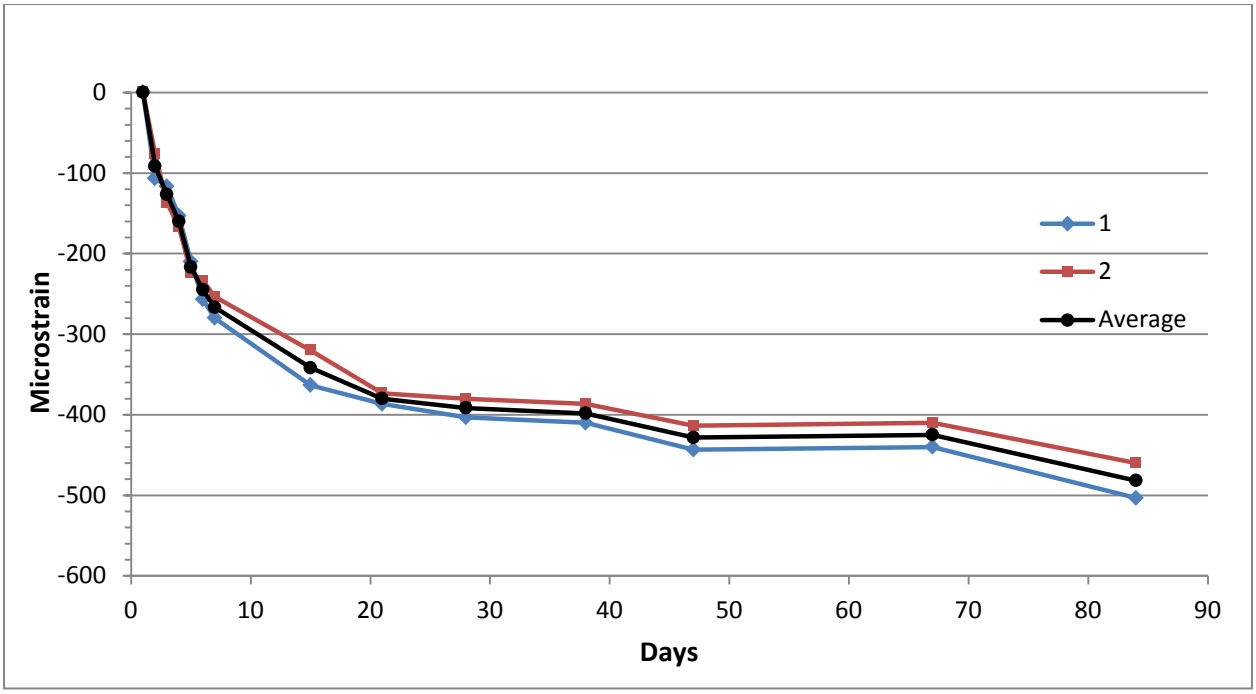

Figure 22 - Unrestrained Shrinkage Strain for SLWA

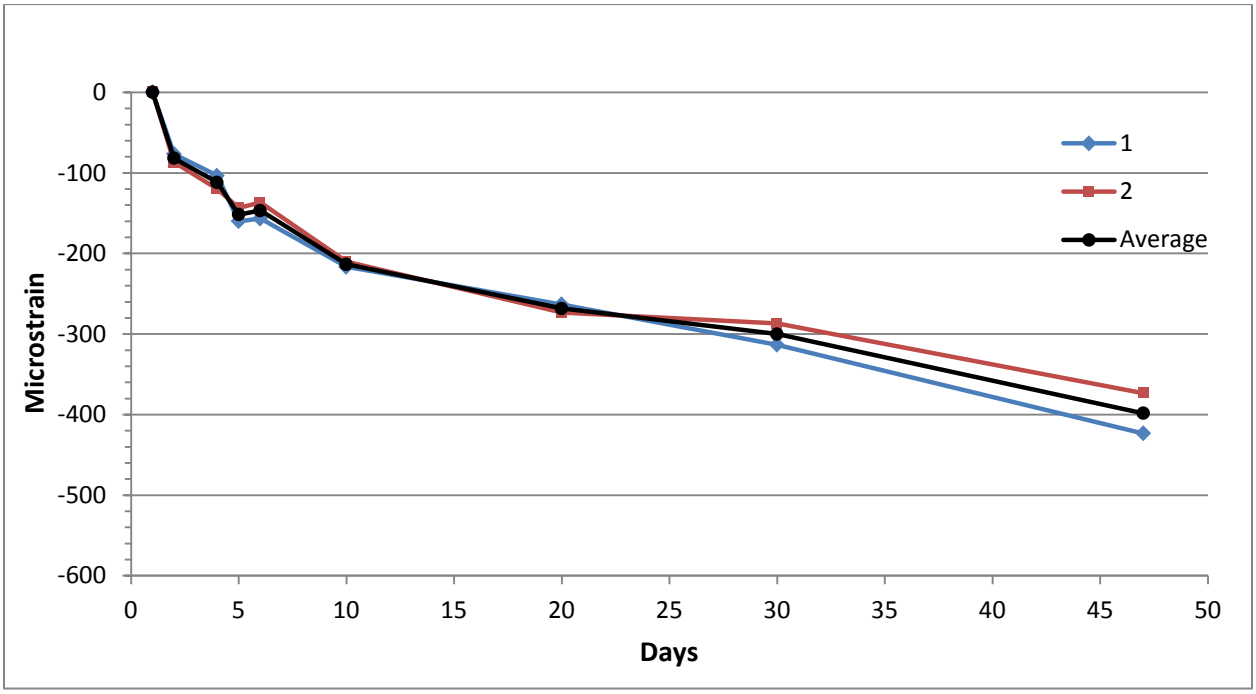

Figure 23 - Unrestrained Shrinkage Strain for Slag

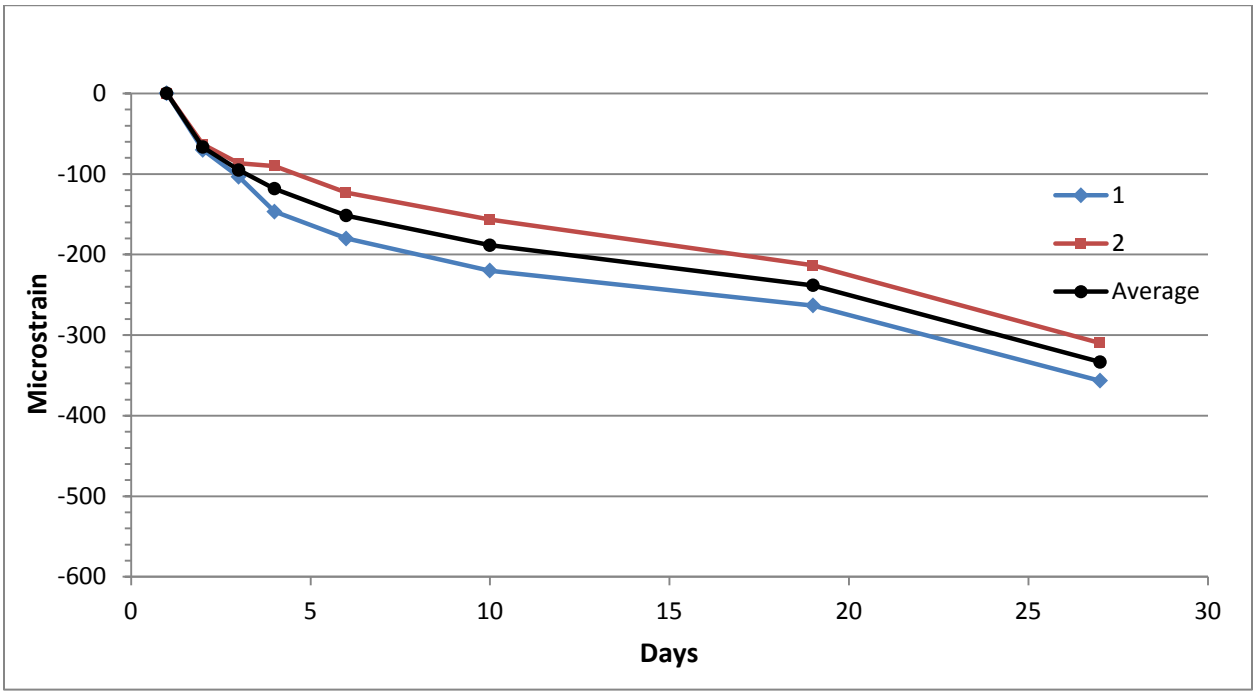

Figure 24 - Unrestrained Shrinkage Strain for SLWA/Slag

The results of comparisons of the AASHTO, ACI 209, CEB MC90, and Bazant B3 models to shrinkage test data from NW-FA 1-3 are shown in Figures 25-27.

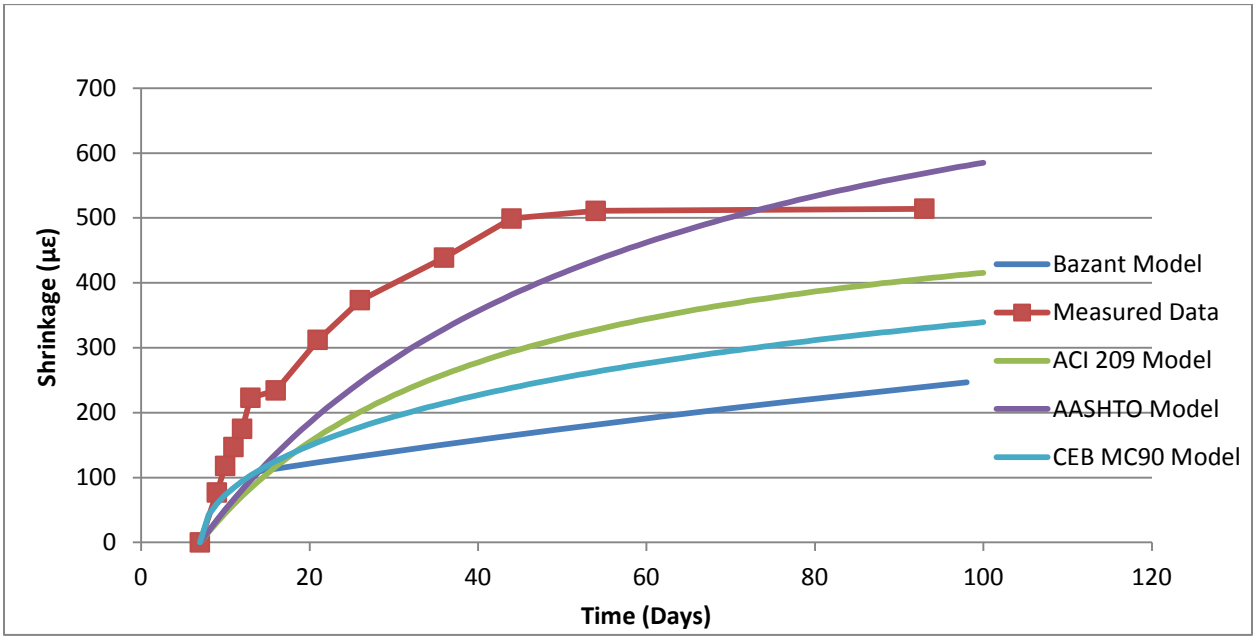

Figure 25 - NW-FA 1 Vs. Shrinkage Models

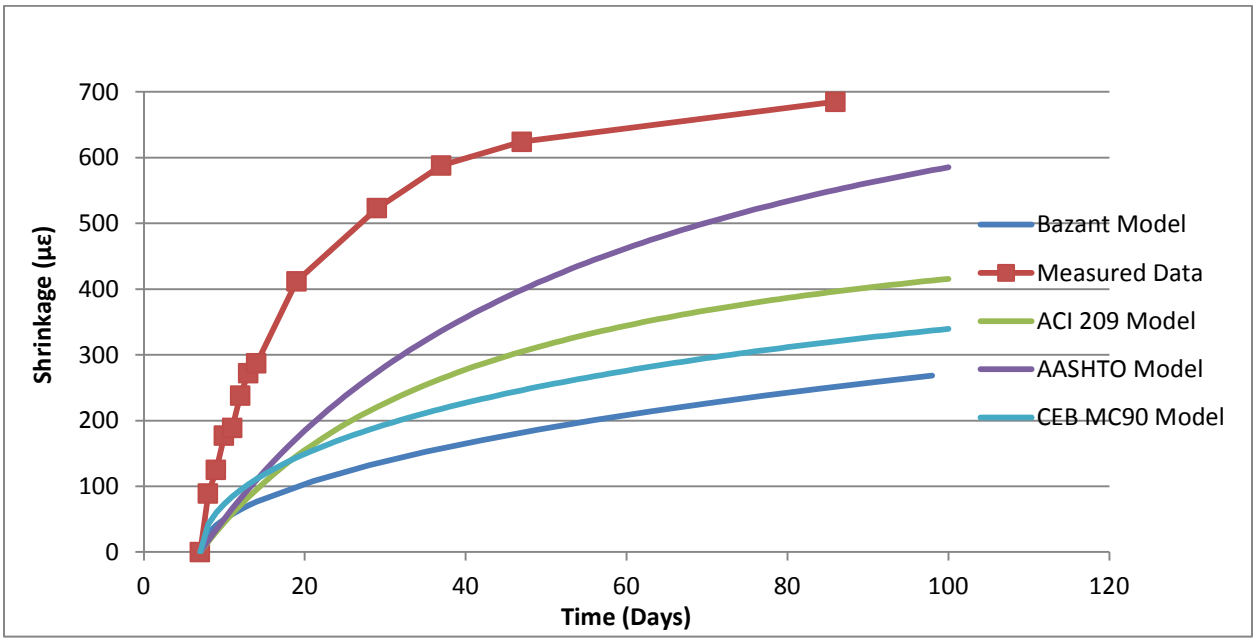

Figure 26 - NW-FA 2 Vs. Shrinkage Models

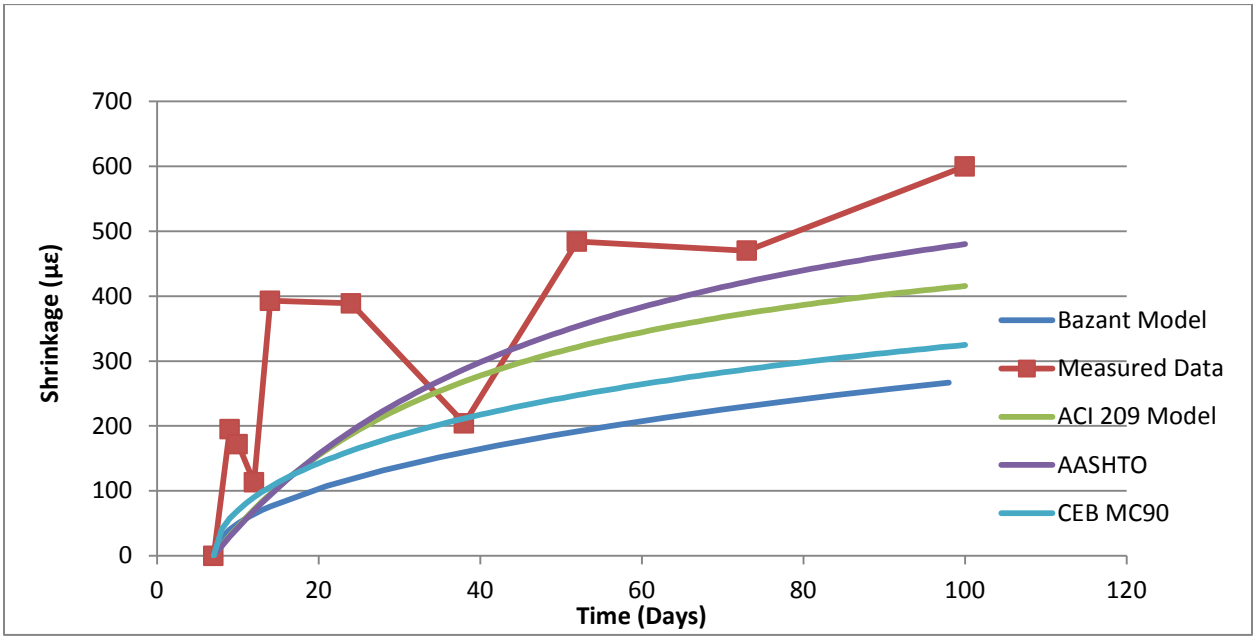

Figure 27 - NW-FA 3 Vs. Shrinkage Models

The results of comparisons of the AASHTO, ACI 209, CEB MC90, and Bazant B3 models to shrinkage test data from SLWA, Slag, and SLWA/Slag mixes are shown in Figures 28-30.

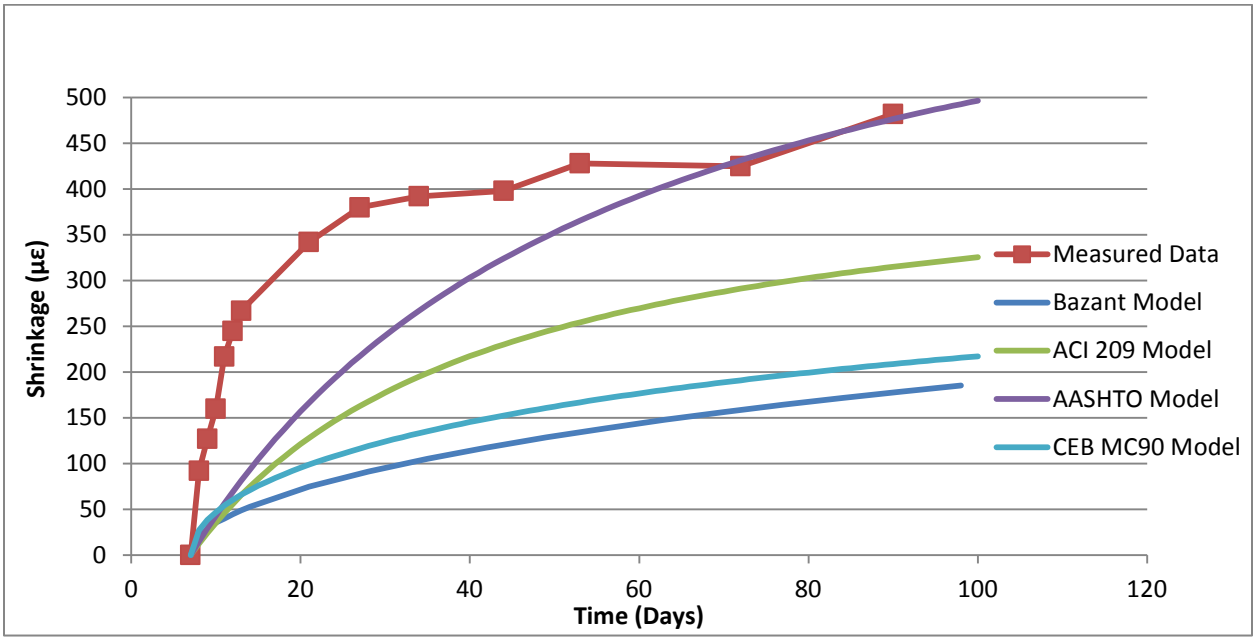

Figure 28 - SLWA Vs. Shrinkage Models

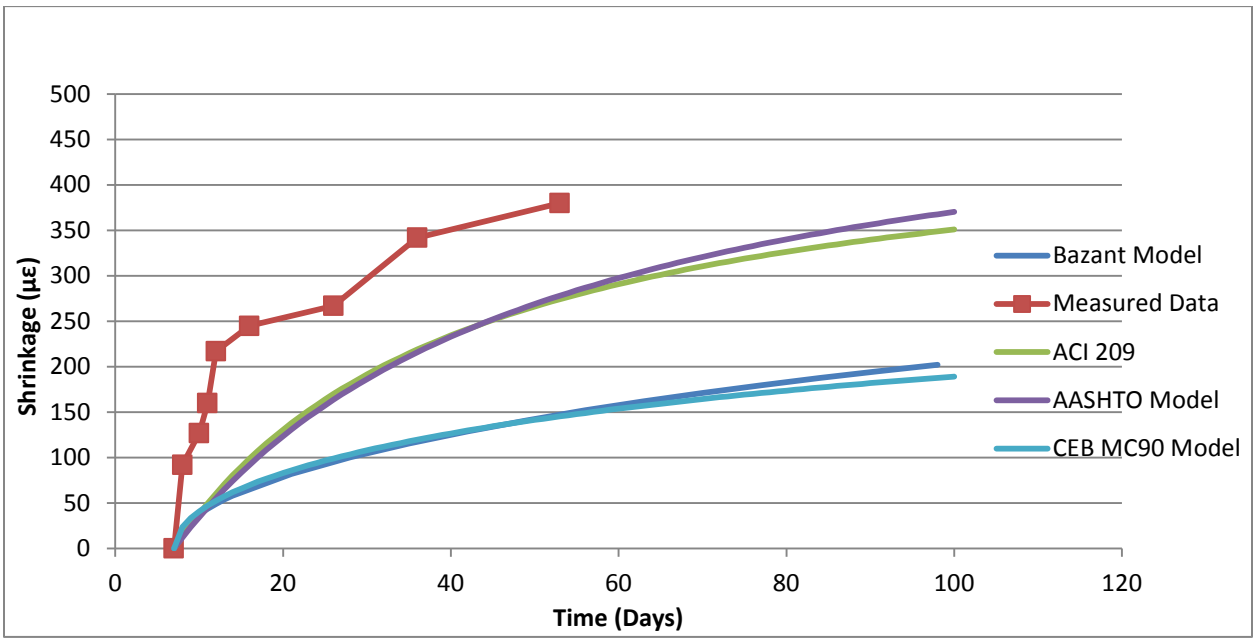

Figure 29 - Slag Vs. Shrinkage Models

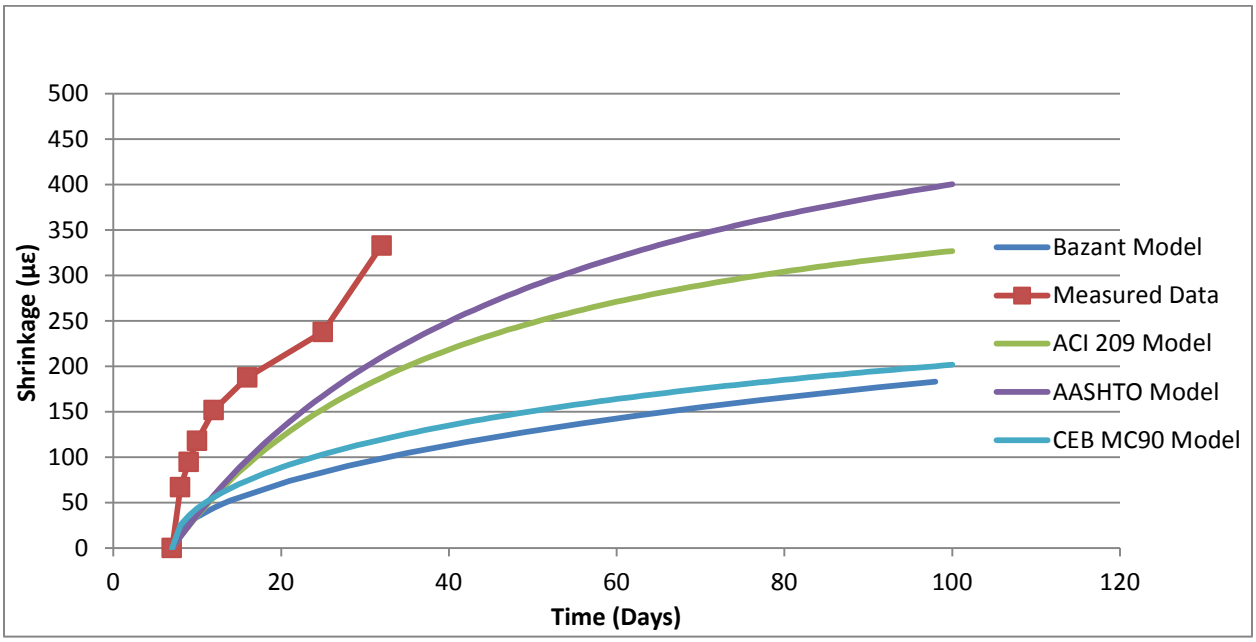

Figure 30 - SLWA/Slag Vs Shrinkage Models

4.4 Compressive Creep

The results of compressive creep testing on NW-FA Mixes 1-3 are presented in the Figures 31-33.

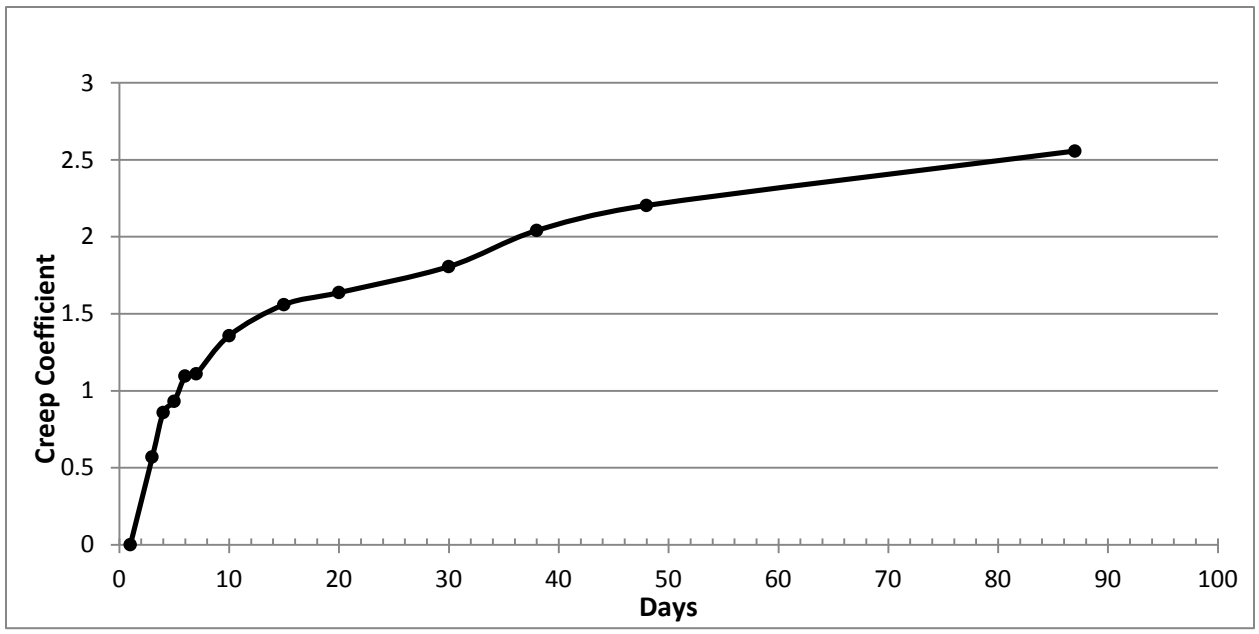

Figure 31 - Creep Coefficient for NW-FA 1

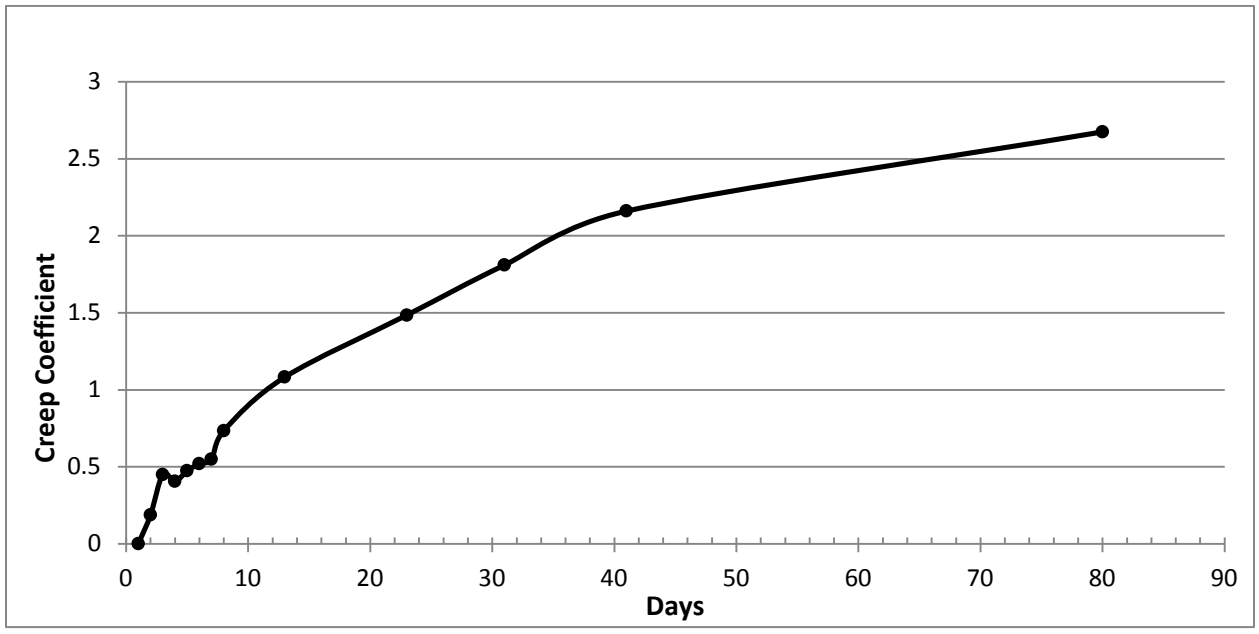

Figure 32 - Creep Coefficient for NW-FA 2

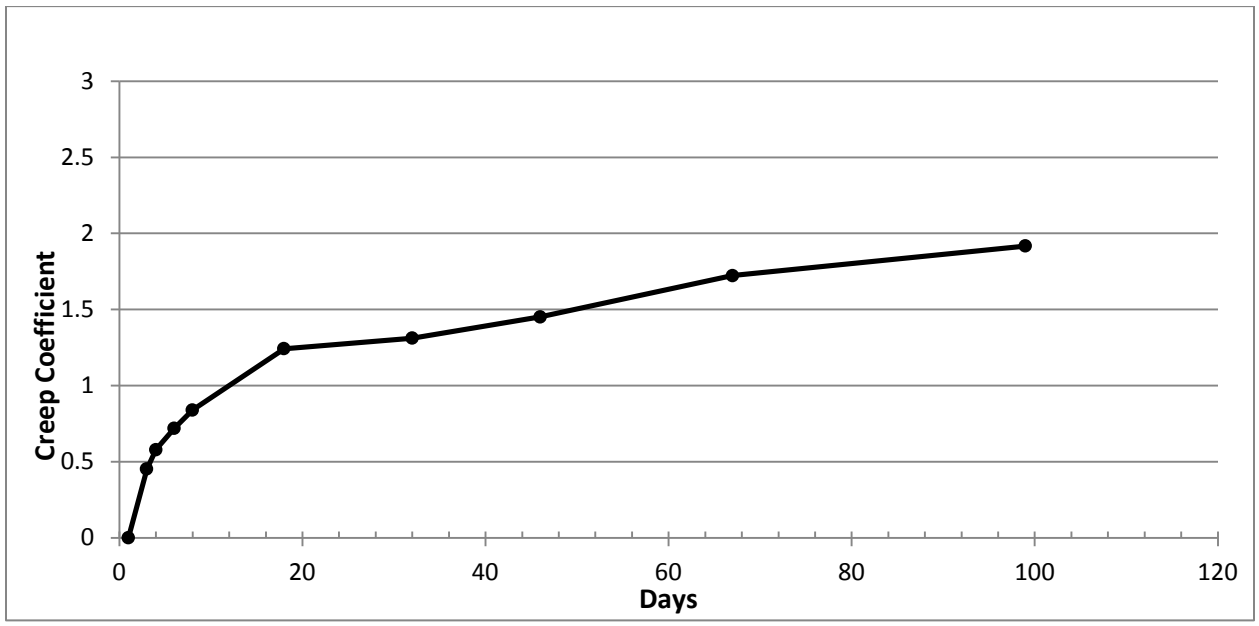

Figure 33 - Creep Coefficient for NW-FA 3

The results of compressive creep testing on SLWA, Slag, and SLWA/Slag mixes are presented in Figures 34-36.

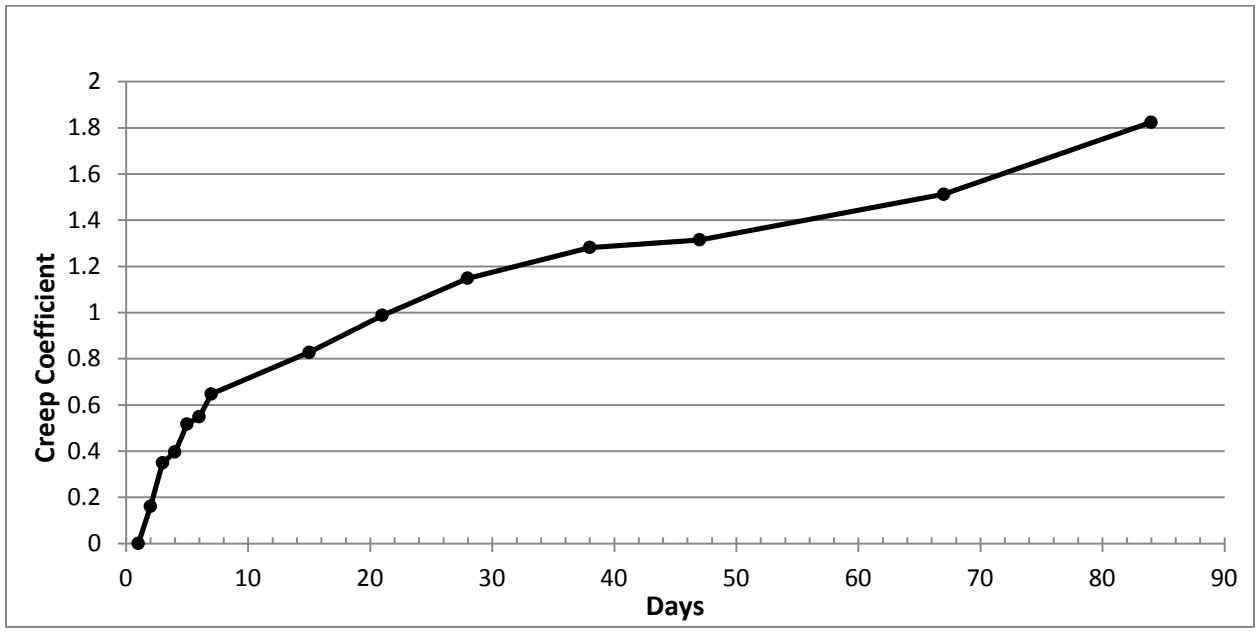

Figure 34 - Creep Coefficient for SLWA

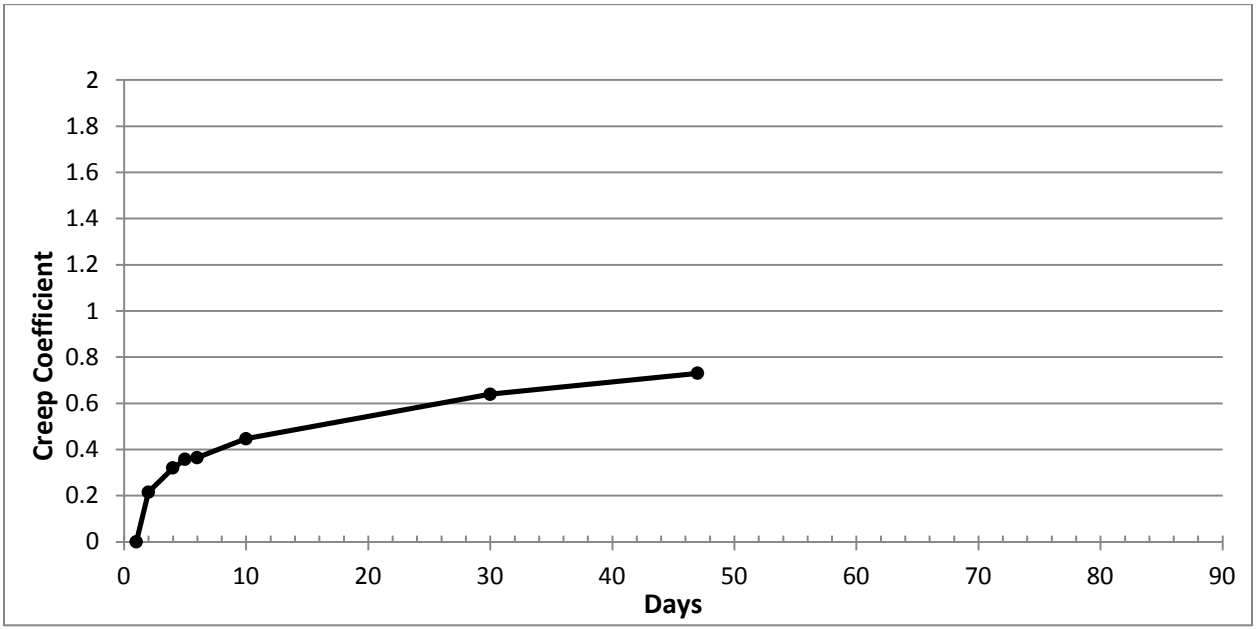

Figure 35 - Creep Coefficient for Slag

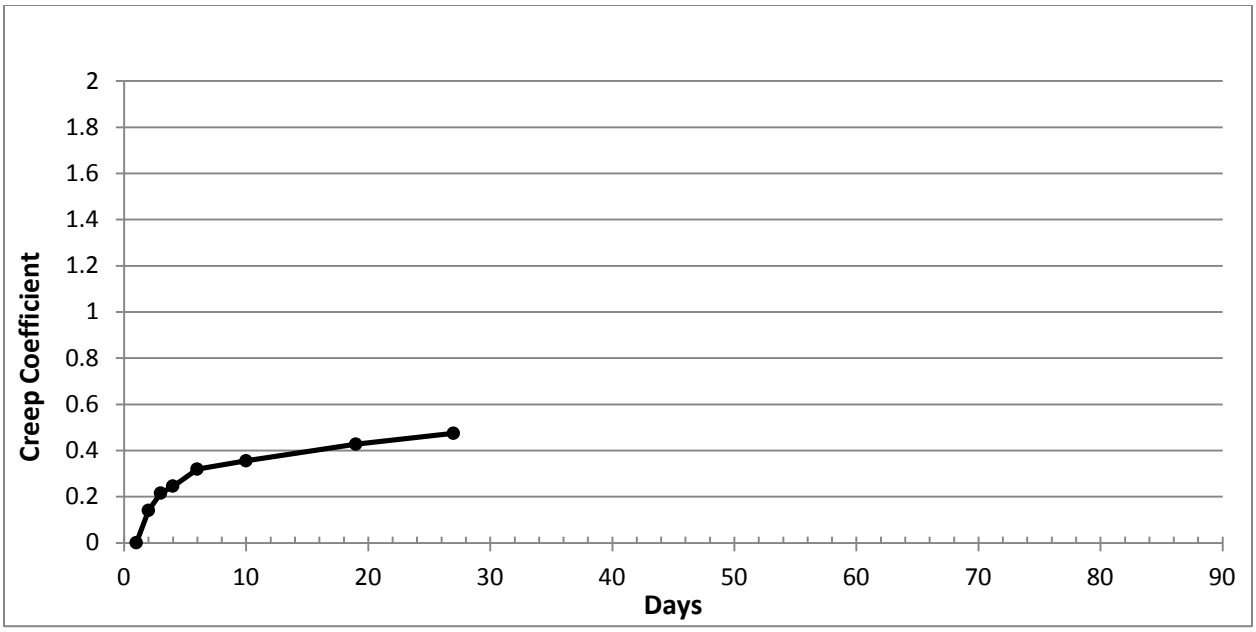

Figure 36 - Creep Strain for SLWA/Slag

The results of comparisons of the AASHTO, ACI 209, CEB MC90, and Bazant B3 models to compressive creep test data from NW-FA mixes 1-3 are shown in Figures 37-39.

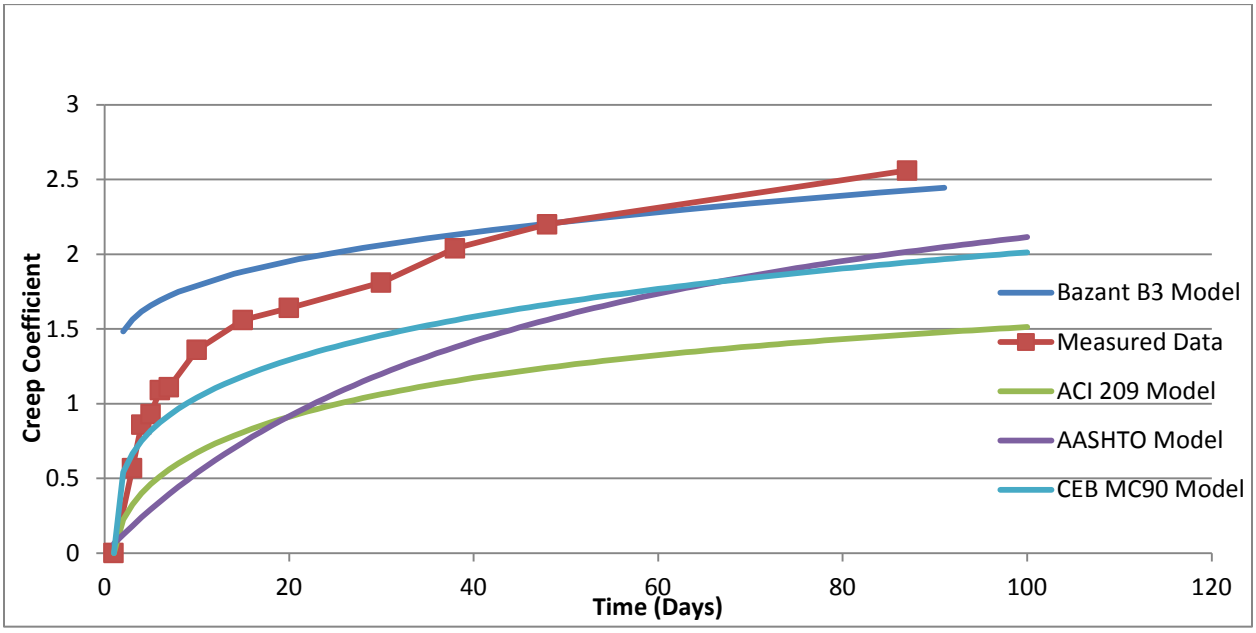

Figure 37 - NW-FA 1 Vs. Creep Models

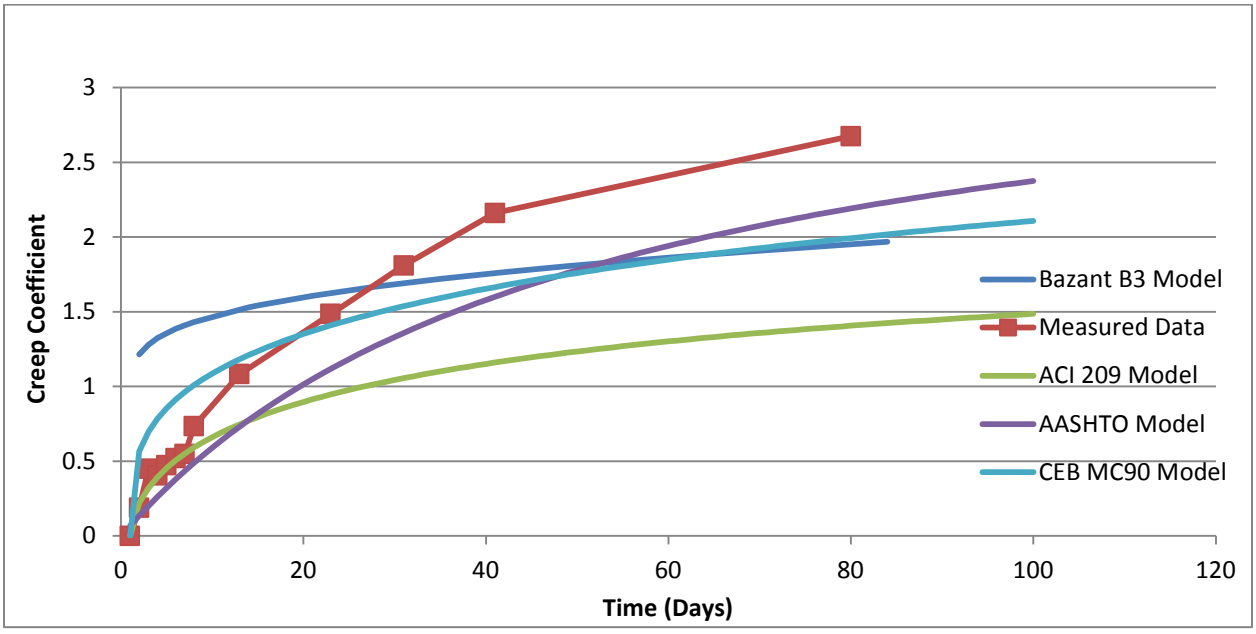

Figure 38 - NW-FA 2 Vs. Creep Models

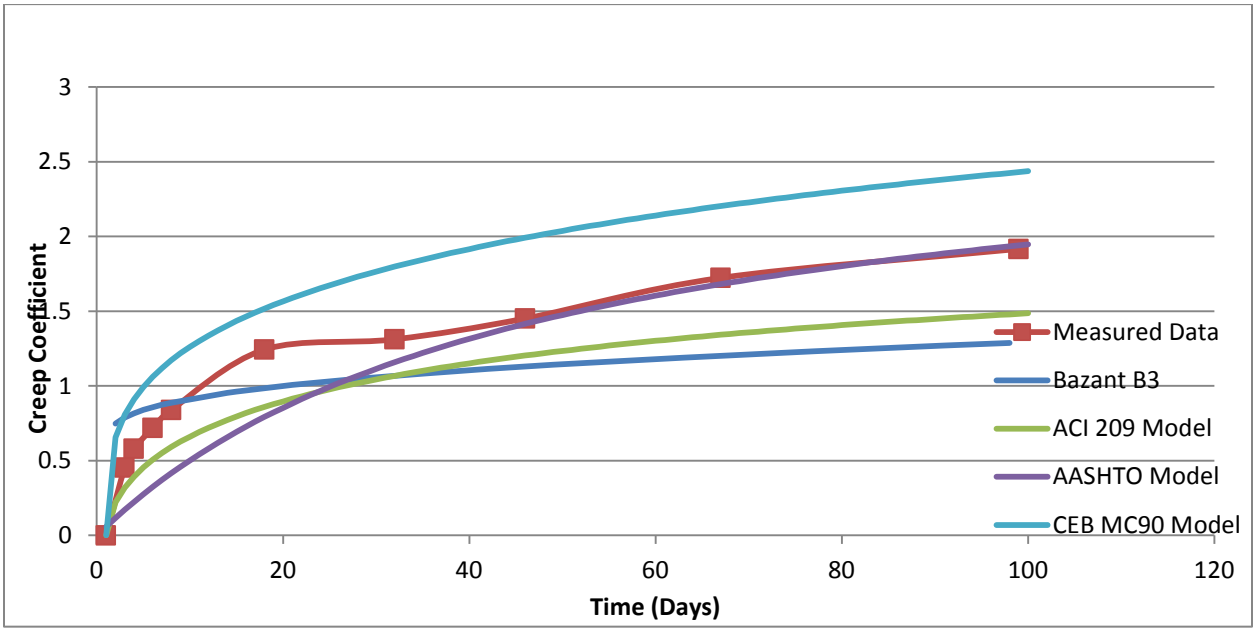

Figure 39 - NW-FA 3 Vs. Creep Models

The results of comparisons of the AASHTO, ACI 209, CEB MC90, and Bazant B3 models to compressive creep test data from SLWA, Slag, and SLWA/Slag mixes are shown in Figures 40-42.

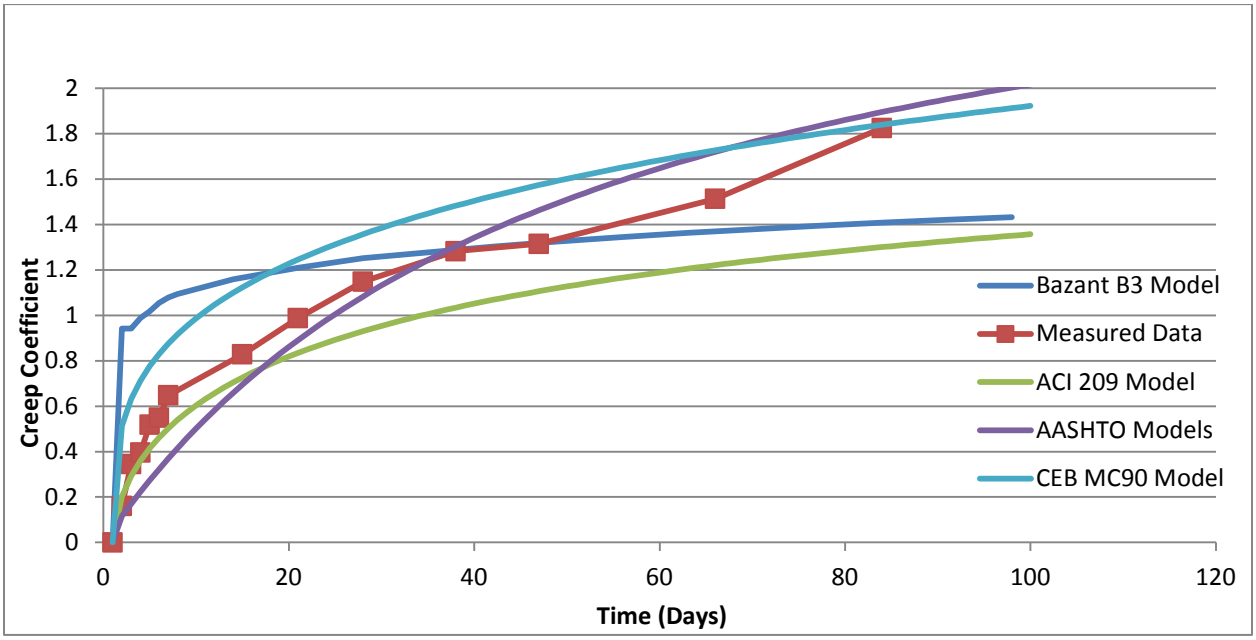

Figure 40 - SLWA Vs. Creep Models

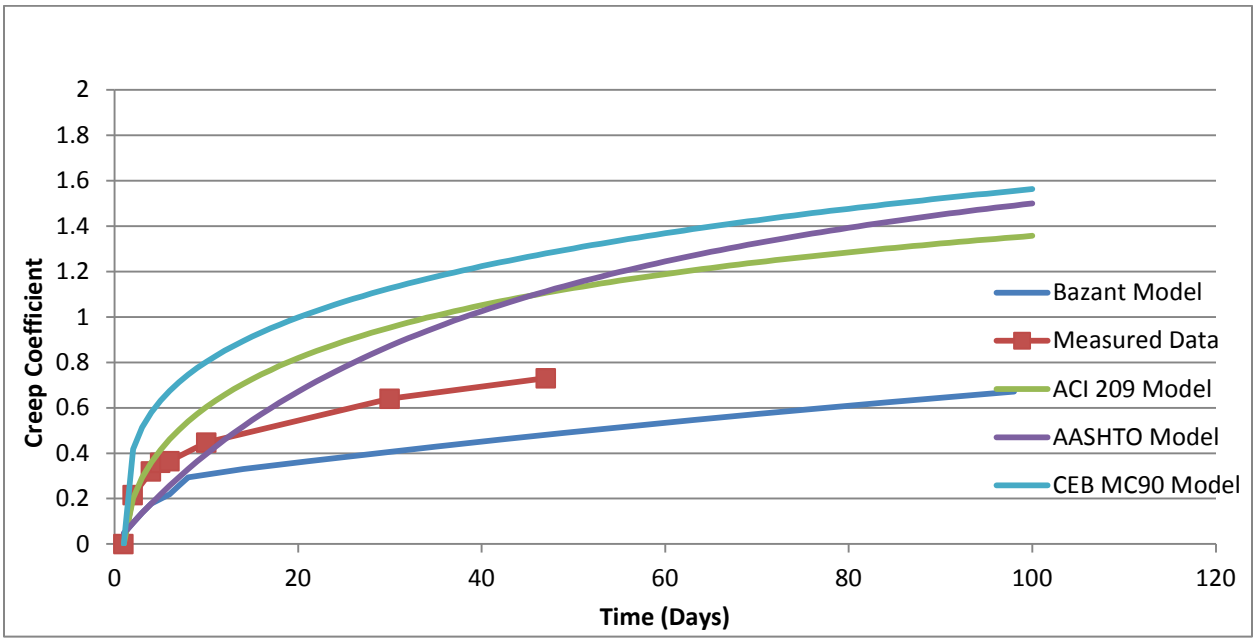

Figure 41 - Slag Vs. Creep Models

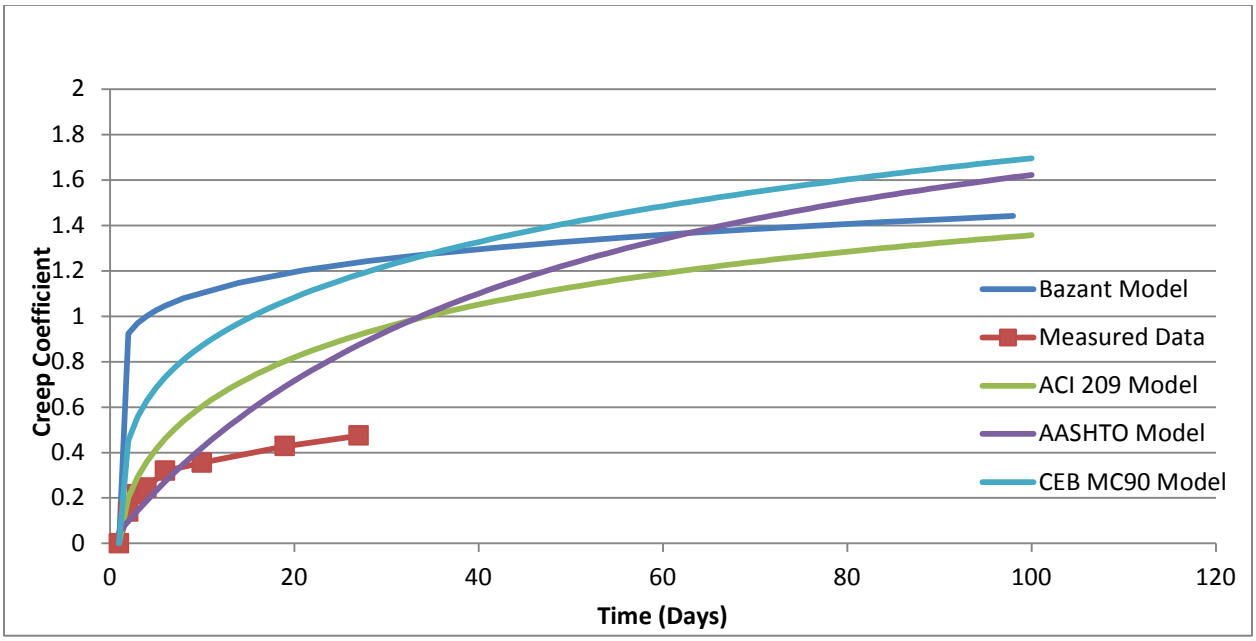

Figure 42 - SLWA/Slag Vs. Creep Models

4.5 Modulus of Elasticity

The results of modulus of elasticity tests on NW-FA mixes 1-3 are shown in Table 20.

Table 20 - NW-FA 1-3 Modulus of Elasticity Results

Specimen Age (Days)	Modulus of Elasticity Test Results (ksi)					
	NW-FA 1	NW-FA 1 Avg.	NW-FA 2	NW-FA 2 Avg.	NW-FA 3	NW-FA 3 Avg.
7	4120	4115	3040	3050	3760	4070
7	4110		3060		4380	
14	2980	3150	3690	3705	3990	4130
14	3320		3720		4270	
28	4140	4190	3060	3110	4260	4025
28	4240		3160		3790	
56	N/A	N/A	N/A	N/A	4020	N/A
56	N/A		N/A		3670	

The results of modulus of elasticity tests on SLWA, Slag, and SLWA/Slag are shown in Table 21.

Table 21 - SLWA, Slag, and SLWA/Slag Modulus of Elasticity Results

Specimen Age (Days)	Modulus of Elasticity Test Results (ksi)					
	SLWA	SLWA Avg.	Slag	Slag Avg.	SLWA/Slag	SLWA/Slag Avg.
7	3690	3510	5150	4840	3860	3695
7	3330		4530		3530	
14	4420	4295	4800	4960	3570	3385
14	4170		5120		3200	
28	4130	3990	5640	5460	4260	4160
28	3850		5280		4060	
56	4800	4670	4860	4950	N/A	N/A
56	4530		5040		N/A	

4.6 Unit Weight of Fresh Concrete

The results of unit weight measurements for SLWA, Slag, and SLWA/Slag mixtures are shown in Table 22.

Table 22 - Unit Weight of Fresh Concrete

Mixture	Unit Weight (lb/ft^3)
SLWA	135
Slag	145
SLWA/Slag	134

4.6 Splitting Tensile Strength

The results of splitting tensile strength tests on NW-FA mixes 1-3 are shown in Table 23.

Table 23 - NW-FA 1-3 Splitting Tensile Strength Test Results

Specimen Age (Days)	Splitting Tensile Strength Test Results (psi)					
	NW-FA 1	NW-FA 1 Avg.	NW-FA 2	NW-FA 2 Avg.	NW-FA 3	NW-FA 3 Avg.
7	350	357	290	280	450	493
7	350		280		510	
7	370		270		520	
28	410	437	360	357	460	430
28	450		350		420	
28	450		360		410	

The results of splitting tensile strength tests on SLWA, Slag, and SLWA/Slag mixes are shown in Table 24.

Table 24 - SLWA, Slag, and SLWA/Slag Splitting Tensile Strength Test Results

Specimen Age (Days)	Splitting Tensile Strength Test Results (psi)					
	SLWA	SLWA Avg.	Slag	Slag Avg.	SLWA/Slag	SLWA/Slag Avg.
7	310	287	460	417	310	377
7	240		370		370	
7	310		420		450	
14	390	320	490	503	450	510
14	290		490		510	
14	280		530		570	
28	470	340	540	483	420	370
28	280		450		350	
28	270		460		340	
56	490	380	410	457	N/A	N/A
56	330		510		N/A	
56	320		450		N/A	

4.7 Tensile Creep

The results of tensile creep tests on SLWA, Slag, and SLWA/Slag tests are shown in Figures 43-45. Note that the high values of tensile creep for the SLWA mix are due to elastic strain being 33% of the expected value, leading to a threefold increase in the creep coefficient. This increase has been accounted for and is further discussed in Chapter 5.

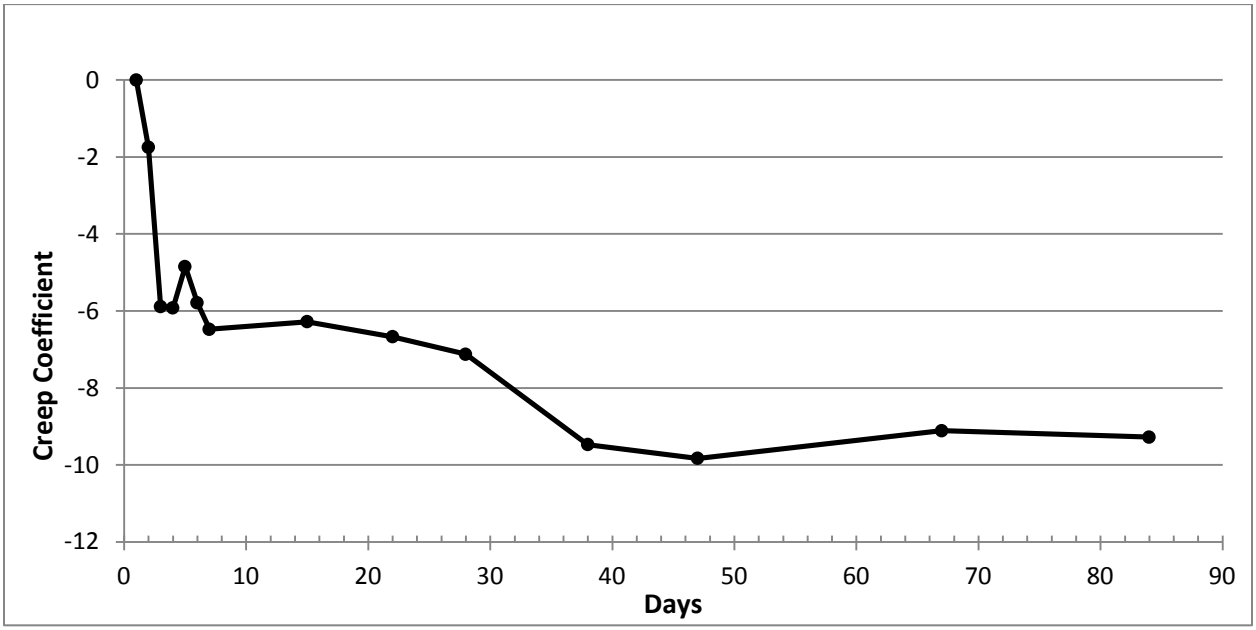

Figure 43 - SLWA Tensile Creep Coefficient

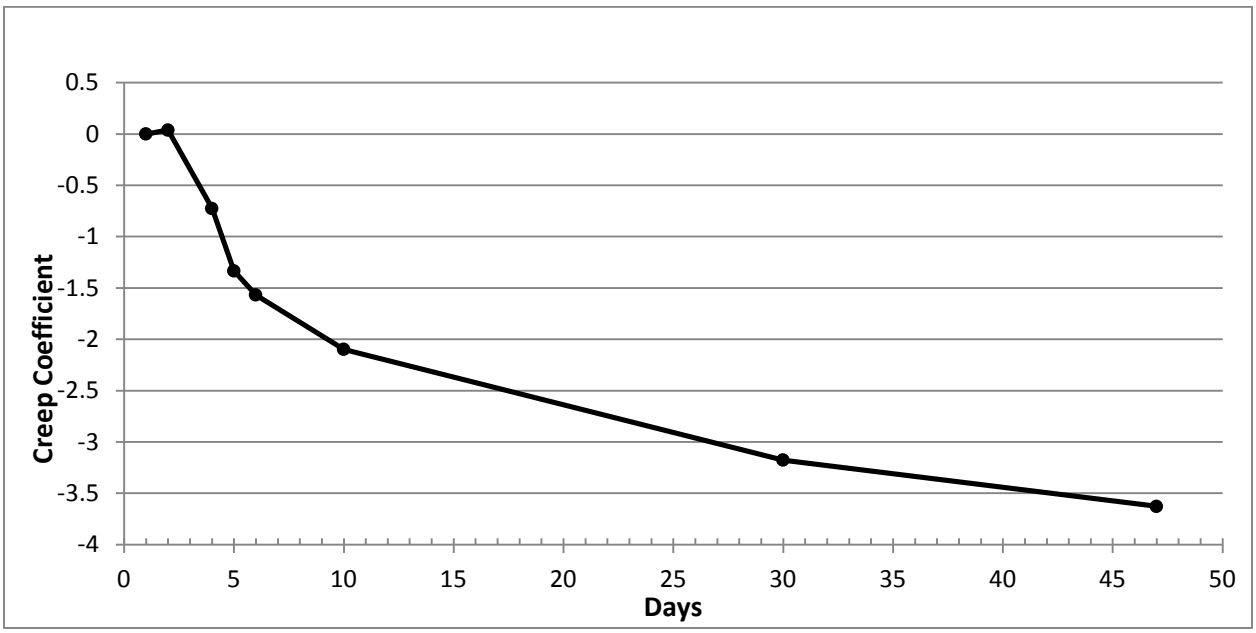

Figure 44 - Slag Tensile Creep Coefficient

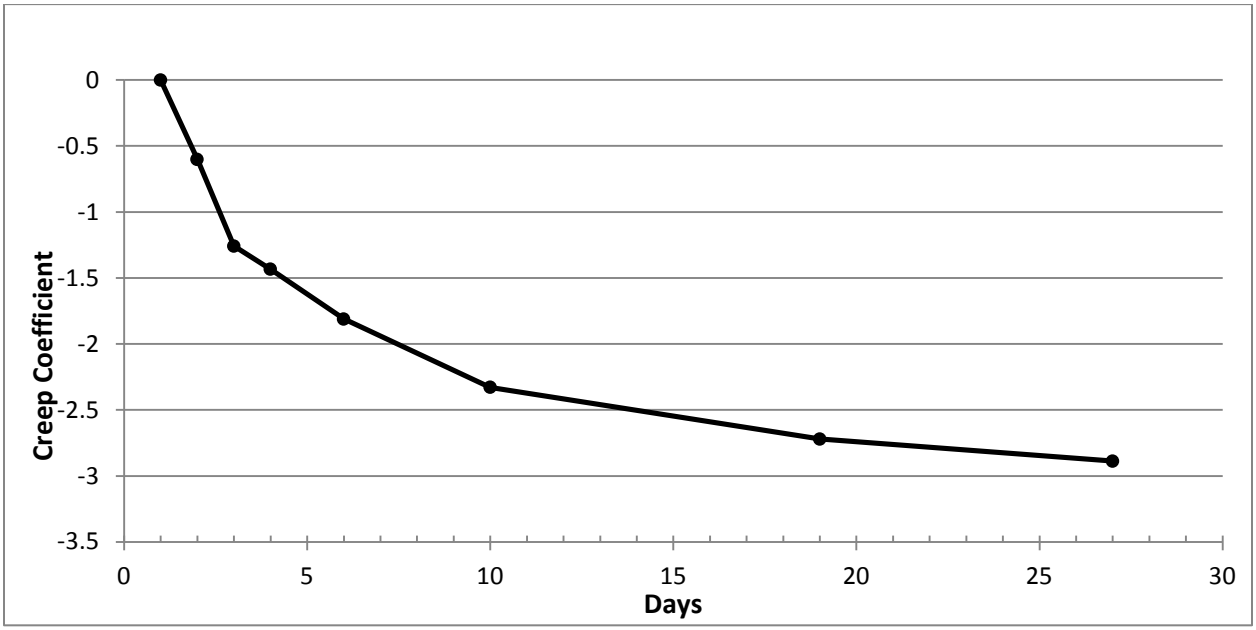

Figure 45 - SLWA/Slag Tensile Creep Coefficient

4.8 Age Adjusted Effective Modulus Parametric Study

The results of the AAEM parametric study to determine the effects of reducing shrinkage and increasing creep are shown in Tables 25 and 26. The values of shrinkage and creep were adjusted to determine their overall effects on the stresses due to differential shrinkage experienced by the composite system. Positive stress is tensile, negative stresses are compressive. All stress values are in ksi. The assumptions and procedure for this method can be found in Chapters 1 and 2. Input values are shown in below. All initial forces are considered to be zero (i.e. the section is unloaded). The age of the beam is taken as 28 days (creep and shrinkage values are taken from material testing results from beam age 28 days to 90 days).

Input Values

$n = 1.41$
$E_D = 3605$ ksi
$E_G = 5100$ ksi
$E_{rebar} = 29000$ ksi
$A_D = 336$ in^2
$A_G = 864$ in^2
$A_{rebar} = 0.598$ in^2
$a = 12.5$ in
$a_D = 9$ in
$a_G = 3.5$ in
$I_D = 1372$ in^4
$I_G = 23328$ in^4
$\varphi_D = 2.16$
$\varphi_G = 1.21$
$\varepsilon_{sD} = 610$ με
$\varepsilon_{sG} = 128$ με
$\mu = 0.7$

Table 25 - Results of AAEM Parametric Study, Part 1

Stress Profile (ksi) at Tapered Section With Default Creep & Shrinkage Values	
Stress at top of deck	0.247
Stress at bottom of deck	0.457
Stress at top of girder	-0.691
Stress at bottom of girder	0.418
Decrease Shrinkage by 10%	
Stress Profile at Tapered Section, CIP Deck 7 in, Precast Girder 18 in.	
Stress at top of deck	0.217
Stress at bottom of deck	0.401
Stress at top of girder	-0.607
Stress at bottom of girder	0.366
Increase Creep by 10%	
Stress Profile at Tapered Section, CIP Deck 7 in, Precast Girder 18 in.	
Stress at top of deck	0.246
Stress at bottom of deck	0.438
Stress at top of girder	-0.673
Stress at bottom of girder	0.407
Decrease Shrinkage by 5%, Increase Creep by 5%	
Stress Profile at Tapered Section, CIP Deck 7 in, Precast Girder 18 in.	
Stress at top of deck	0.232
Stress at bottom of deck	0.42
Stress at top of girder	-0.64
Stress at bottom of girder	0.387

Table 26 - Results of AAEM Parametric Study, Part 2

Decrease Shrinkage by 15%	
Stress Profile at Tapered Section, CIP Deck 7 in, Precast Girder 18 in.	
Stress at top of deck	0.202
Stress at bottom of deck	0.373
Stress at top of girder	-0.565
Stress at bottom of girder	0.341
Increase Creep by 15%	
Stress Profile at Tapered Section, CIP Deck 7 in, Precast Girder 18 in.	
Stress at top of deck	0.245
Stress at bottom of deck	0.43
Stress at top of girder	-0.664
Stress at bottom of girder	0.402
Decrease Shrinkage by 7.5%, Increase Creep by 7.5%	
Stress Profile at Tapered Section, CIP Deck 7 in, Precast Girder 18 in.	
Stress at top of deck	0.224
Stress at bottom of deck	0.402
Stress at top of girder	-0.615
Stress at bottom of girder	0.372
Decrease Shrinkage by 15%, Decrease Creep by 5%	
Stress Profile at Tapered Section, CIP Deck 7 in, Precast Girder 18 in.	
Stress at top of deck	0.202
Stress at bottom of deck	0.381
Stress at top of girder	-0.573
Stress at bottom of girder	0.346
Decrease Shrinkage by 15%, Decrease Creep by 10%	
Stress Profile at Tapered Section, CIP Deck 7 in, Precast Girder 18 in.	
Stress at top of deck	0.202
Stress at bottom of deck	0.39
Stress at top of girder	-0.58
Stress at bottom of girder	0.35

These results suggest that reducing shrinkage has the greatest effect on reducing stresses in the composite cross-section, even if this results in decreasing creep.

CHAPTER 5: DISCUSSION AND ANALYSIS

This chapter presents a discussion of the test results found in chapter 4, including compressive strength, unrestrained shrinkage, compressive creep, modulus of elasticity, splitting tensile strength, and tensile creep.

5.1 Compressive Strength

Table 27 summarizes results of compressive strength tests performed during the course of this research project.

Table 27 - Average Compressive Strength of 4x8 Cylinders

Average Compressive Strength of 4x8 Cylinders (psi)						
Age (days)	NW-FA 1	NW-FA 2	NW-FA 3	SLWA	Slag	SLWA/Slag
7	3110	2610	3500	2650	4100	3660
14	3340	3340	4100	3280	4830	4130
28	3810	3380	4000	3540	5370	4560
56	N/A	N/A	3980	3610	5410	N/A
90	N/A	N/A	N/A	N/A	N/A	N/A

5.1.1 Normal Weight Fly Ash Mixtures

Fly ash is used as an admixture in PCC as a partial replacement for Portland cement. Its general effect is to increase later age strength. However, it also causes reduction in early age strength, which can be seen in the compressive strength results as the mixtures utilizing fly ash did not achieve the specified 4 ksi at 28 days of age (with the exception of NW-FA Mix 3, which achieved 4 ksi at 14 days. This early age strength is most likely due to a lack of air entrainment in this mixture. The material otherwise performed as expected, showing similar values at different ages.

5.1.2 SLWA, Slag, and SLWA/Slag Mixtures

As would be expected, the inclusion of SLWA resulted in decreased compressive strengths at all ages of the concrete mixture. The SLWA has reduced density when compared to normal weight sand and thus results in reduced strength.

The mixture utilizing a 40% replacement by weight of NEWCEM Slag cement achieved very high early strengths, more so than would be expected. This was also noted by Mokarem (Mokarem 2002). The inclusion of slag cement may assist with the reduction in strength due to the addition of SLWA.

The SLWA/Slag mixture, as expected, achieved a compressive strength in between the values found in the SLWA and Slag mixtures. If additional strength is needed as requested by the designer, test results show that slag cement is a viable option.

5.2 Unrestrained Shrinkage

Table 28 summarizes results of unrestrained shrinkage at 28 and 90 days age for tests performed during the course of this research project.

Table 28 - Unrestrained Shrinkage Values

Unrestrained Shrinkage Values (με)						
Age (days)	NW-FA 1	NW-FA 2	NW-FA 3	SLWA	Slag	SLWA/Slag
28	373	523	389	380	268	280
90	514	685	600	482	N/A	N/A

5.2.1 Normal Weight Fly Ash Mixtures

With the exception of NW-FA mix 3 (due to a malfunctioning environmental chamber), the NW-FA mixtures experienced similar unrestrained shrinkage values. NW-FA Mix 1 incorporated

the results from three unrestrained shrinkage prisms. One of the three shrinkage prisms experienced unrealistic values of shrinkage (approximately three times as much as the others). This outlier shrinkage data was disregarded – it is unknown as to why the values were escalated. When compared against shrinkage models, the AASHTO shrinkage model found in the LRFD Bridge Design Specification most accurately described the behavior of the concrete mixture. The ACI 209 and CEB MC90 models typically under-predicted the amount of shrinkage experienced by the concrete mixture, as did the Bazant B3 shrinkage model (to a greater degree than ACI and CEB).

5.2.2 SLWA, Slag, and SLWA/Slag Mixtures

The SLWA mixture experienced normal values of shrinkage until the age of approximately 14 days, at which time shrinkage was significantly retarded due to the availability of water within the SLWA. However, at later ages, shrinkage accelerated again. Future work in this area would benefit from increasing the amount of SLWA utilized in order to provide the internal curing needed to continue to retard shrinkage throughout the curing process of the concrete mixture. The Slag mix experienced normal values of shrinkage (when compared against NW-FA mixtures). Test results show that the addition of Slag cement into a 4 ksi mixture do not have an effect on shrinkage. However, the sample size is not large enough to make any definitive statements in this area. The SLWA/Slag mixture also seems to share the benefits experienced by the SLWA mixture as at an age of 28 days the SLWA/Slag mixture appears to be undergoing reduced shrinkage when compared against the NW-FA mixtures. Further monitoring of this mix is required in order to determine whether internal curing will be sufficient to retard shrinkage as seen in the SLWA mix. When compared against the shrinkage models, all four models vastly

under-predict shrinkage. During the monitoring process, the environmental chamber humidity values increased to 80%. It seems apparent that the current shrinkage models have difficulty predicting shrinkage values when humidity values increase above that which is normally experienced in the field and/or normal laboratory conditions. Of the four models, the AASHTO shrinkage model most closely predicted values for shrinkage strain.

5.3 Compressive Creep

Table 29 summarizes results of unrestrained shrinkage at 28 and 90 days age for tests performed during the course of this research project.

Table 29 - Compressive Creep Coefficient Values

Compressive Creep Coefficient Values						
Age (days)	NW-FA 1	NW-FA 2	NW-FA 3	SLWA	Slag	SLWA/Slag
28	1.81	1.81	1.31	1.15	0.64	0.47
90	2.56	2.68	1.92	1.82	N/A	N/A

5.3.1 Normal Weight Fly Ash Mixtures

All of the NW-FA mixtures experienced similar values of compressive creep. When compared against creep models, the ACI model generally showed the best correlation at early ages, but under-predicted later age creep. The Bazant model captured later age creep the best of the four models, but over-predicted early age creep. The AASHTO and CEB MC90 models were both fairly accurate throughout the testing process, but were less accurate at early and late ages than the other models.

5.3.2 Slag, SLWA, and SLWA/Slag Mixtures

The SLWA mixture experienced slightly reduced creep coefficient values when compared to the NW-FA mixture. This result is unexpected, considering the reduced compressive strength

and modulus of elasticity. This could be partially explained by the large amount of elastic strain experienced when the specimen was initially loaded. When compared against models, the AASHTO model was the most effective at predicting values for the creep coefficient over time. The ACI and CEB MC90 models either over or under-predicted values of creep and the Bazant model was the least accurate of the four models.

The slag cement mixture experienced highly reduced creep when compared to the NW-FA mixture. This is due to the very high early strength development caused by the introduction of slag cement into the mixture. When compared against creep models, the ACI 209 accurately captured early-age creep but over-predicted mid-late age values. The Bazant model most accurately predicted values throughout the curing process, while the AASHTO and CEB MC90 models significantly over-predicted creep.

The SLWA/slag mixture experienced very little creep when compared to the other mixtures. The reasons for this behavior are unknown. Further monitoring of the mixture is required to make a determination as to the final behavior of this mixture. The AASHTO model accurately predicted early-age creep but over-predicted mid-late age behavior. The other three models significantly over-predicted creep behavior at all ages of the concrete mixture.

5.4 Modulus of Elasticity

Tables 30 and 31 summarize results of modulus of elasticity tests performed during the course of this research project compared against E = $33w_c^{1.5}\sqrt{f'_c}$.

Table 30 - NW-FA 1-3 Modulus of Elasticity Comparisons

Modulus of Elasticity (ksi) Test Vs. E = $33w_c^{1.5}\sqrt{f'_c}$						
Age (Days)	NW-FA 1		NW-FA 2		NW-FA 2	
	Test Value	E = $33w_c^{1.5}\sqrt{f'_c}$	Test Value	E = $33w_c^{1.5}\sqrt{f'_c}$	Test Value	E = $33w_c^{1.5}\sqrt{f'_c}$
7	4110	3180	3050	2910	4070	3400
14	3150	3290	3705	3290	4130	3650
28	4190	3520	3110	3310	4020	3600

Table 31 - SLWA, Slag, and SLWA/Slag Modulus of Elasticity Comparisons

Modulus of Elasticity (ksi) Test Vs. E =$33w_c^{1.5}\sqrt{f'_c}$						
Age (Days)	SLWA		Slag		SLWA/Slag	
	Test Value	E = $33w_c^{1.5}\sqrt{f'_c}$	Test Value	E = $33w_c^{1.5}\sqrt{f'_c}$	Test Value	E = $33w_c^{1.5}\sqrt{f'_c}$
7	3510	2640	4840	3520	3700	3080
14	4300	2930	4960	3830	3390	3270
28	3990	3060	5460	4030	4160	3440
56	4670	3090	4950	4050	N/A	N/A

5.4.1 Normal Weight Fly Ash Mixtures

NW-FA mixtures 1 and 3 show similar stiffness values with good correlation to the compressive strength values given by E = $33w_c^{1.5}\sqrt{f'_c}$. Mixture 2 showed reduced values at the age of 28 days compared to the results from 14 day testing. The reasons for this are unknown, but can be attributed to the inherent variability present in concrete material testing.

5.4.2 SLWA, Slag, and SLWA/Slag Mixtures

SLWA and Slag mixtures show test results which are higher than those predicted by compressive strength values. The SLWA/Slag mix shows good correlation to compressive strength values with no serious outliers or unexpected values.

5.5 Splitting Tensile Strength

Tables 32 and 33 summarize results of modulus of elasticity tests performed during the course of this research project compared against $f'_t = 7.5\sqrt{f'_c}$.

Table 32 - NW-FA 1-3 Splitting Tensile Strength Comparisons

Splitting Tensile Strength (psi) Test Vs. $f'_t = 7.5\sqrt{f'_c}$						
Age (Days)	NW-FA 1		NW-FA 2		NW-FA 2	
	Test Value	$f'_t = 7.5\sqrt{f'_c}$	Test Value	$f'_t = 7.5\sqrt{f'_c}$	Test Value	$f'_t = 7.5\sqrt{f'_c}$
7	357	418	280	380	493	444
28	437	463	357	436	430	474

Table 33 - SLWA, Slag, and SLWA/Slag Splitting Tensile Strength Comparisons

Splitting Tensile Strength (psi) Test Vs. $f'_t = 7.5\sqrt{f'_c}$						
Age (Days)	SLWA		Slag		SLWA/Slag	
	Test Value	$f'_t = 7.5\sqrt{f'_c}$	Test Value	$f'_t = 7.5\sqrt{f'_c}$	Test Value	$f'_t = 7.5\sqrt{f'_c}$
7	287	386	417	479	377	454
14	320	430	503	521	510	482
28	340	446	483	550	370	506
56	380	451	457	552	N/A	N/A

5.5.1 Normal Weight Fly Ash Mixtures

All NW-FA mixtures show tensile strength values with good correlation to compressive strength values given by $f_t = 7.5\sqrt{f'_c}$. There are no serious outliers or unexpected values.

5.5.2 SLWA, Slag, and SLWA/Slag Mixtures

The majority of SLWA, Slag, and SLWA/Slag mixtures show tensile strength values which are lower than those predicted by $f_t = 7.5\sqrt{f'_c}$.

5.6 Tensile Creep

The values for the tensile creep coefficient experienced by the SLWA mixture are highly inflated. This is due to the initial elastic deformation being measured as approximately 30% of what would be expected from Hooke's law. The initial elastic deformation was measured as 10 με rather than the expected 30 με. This could be due to the resolution of the measuring devices being 4 με. In order to avoid this issue in the future, it is recommended that a gauge capable of achieving resolutions of approximately 1με be utilized to provide better precision. Assuming an expected value of initial elastic strain of 30 με, the tensile creep coefficient ends up being approximately 50% more than the compressive creep coefficient.

Values for the tensile creep coefficient for the slag mixture are much higher than the compressive creep coefficient (by a factor of approximately 4). Further readings and testing are required to make a determination as to whether these test results are consistent and repeatable.

Values for the relationship between the tensile and compressive creep coefficient for the SLWA/slag mixture are similar to those of the slag only mixture. Data has only been collected for 28 days at the current time – it remains to be seen as to whether this trend continues throughout the curing process.

It appears that compressive creep and tensile creep are related by a factor of 4-6. See Table 34 for a comparison between the two values. These results do not agree with what is found in the literature (specifically results published by Poston, et al.). However, the sample size found within the scope of this research project is insufficient to draw definitive conclusions.

Table 34 - Tensile and Compressive Creep Coefficient Comparisons

Tensile and Compressive Creep Coefficient Comparisons		
Mix	28 Day Comp. Creep Coefficient	28 Day Tensile Creep Coefficient
SLWA	1.15	7.12
Slag	0.64	3.18
SLWA/Slag	0.474	2.89

CHAPTER 6: CONCLUSIONS AND SUMMARY

6.1 Shrinkage Model Selection

Table 35 shows the shrinkage models which performed the best at early ages, late ages, and overall. In general, the AASHTO model performed the best and should be used in the future to predict shrinkage strain at varying ages of concrete during its curing cycle. All models underestimated shrinkage strain throughout the testing process to varying extents. It appears that these models have difficulty predicting shrinkage strain development at higher humidity values similar to those experienced during the testing procedure (humidity values were held at approximately 80%). All models examined during the testing process have a reduction factor for relative humidity contained within their predictive process and it appears that this reduction factor should be lowered.

Table 35 - Shrinkage Model Selection

Mix	Best Model Early Age	Best Model Late Age	Best Model Overall
NW-FA 1	AASHTO	AASHTO	AASHTO
NW-FA 2	AASHTO	AASHTO	AASHTO
NW-FA 3	CEB MC90	AASHTO	AASHTO
SLWA	AASHTO	AASHTO	AASHTO
Slag	ACI 209	AASHTO	AASHTO
SLWA/Slag	AASHTO	AASHTO	AASHTO

6.2 Compressive Creep Model Selection

Table 36 shows the compressive creep models which performed the best at early ages, late ages, and overall. In general, the ACI 209 model gave the best predictions at early ages but was

much less accurate at later ages. The AASHTO model and Bazant B3 both performed relatively well at later ages, however, the AASHTO model was the best overall due to the Bazant B3 model not performing well at early ages. All models severely under predicted creep for the SLWA, Slag, and SLWA/Slag mixes. This is due to the reduced drying shrinkage experienced by these mixes leading to reduced drying creep.

Table 36 - Creep Model Selection

Mix	Best Model Early Age	Best Model Late Age	Best Model Overall
NW-FA 1	CEB MC90	Bazant B3	Bazant B3
NW-FA 2	ACI 209	AASHTO	AASHTO
NW-FA 3	CEB MC90	AASHTO	AASHTO
SLWA	ACI 209	CEB MC90	AASHTO
Slag	ACI 209	Bazant B3	Bazant B3
SLWA/Slag	ACI 209	None	None

6.3 Unrestrained Shrinkage Conclusions

Figure 46 shows the results of unrestrained shrinkage tests performed during the course of the research project. The shrinkage values from the three NW-FA mixes have been averaged in order to compare against the shrinkage values obtained from testing the SLWA, Slag, and SLWA/Slag mixtures.

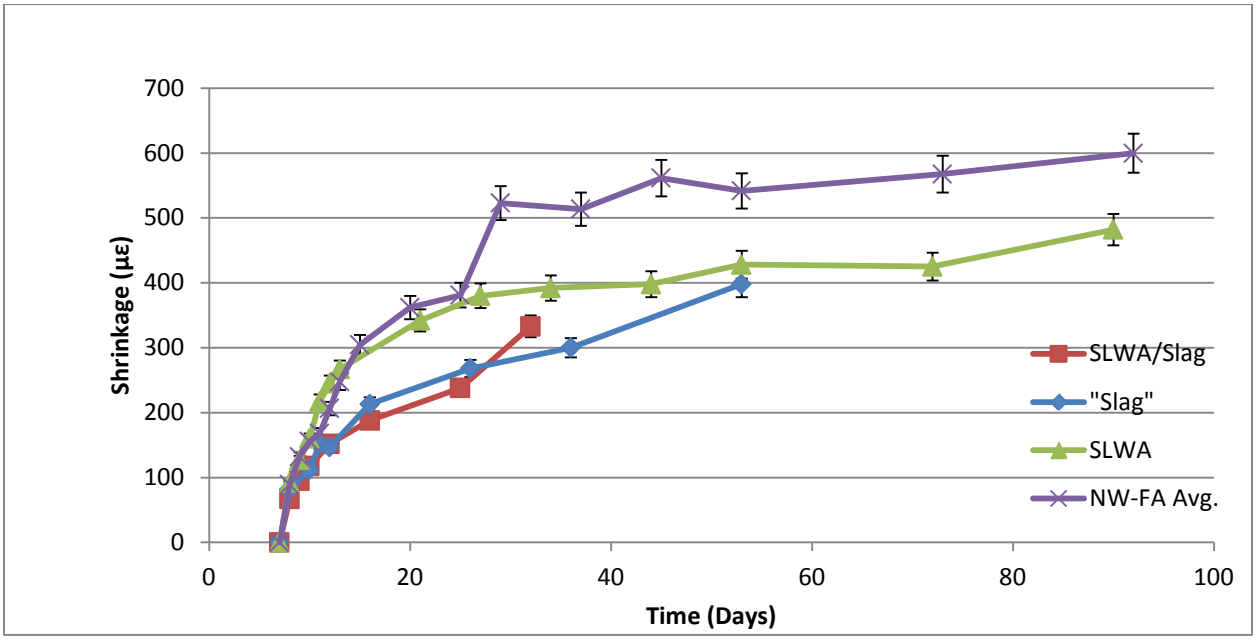

Figure 46 - Unrestrained Shrinkage for NW-FA Avg. Vs. SLWA, Slag, and SLWA/Slag

It can be seen that the NW-FA mixture performed approximately the same as the SLWA mixture until approximately 25 days at which point unrestrained shrinkage continued to increase. The SLWA mixture experienced very little shrinkage past 25 days compared to the NW-FA mixtures. Although complete data is not available for the Slag and SLWA/Slag mixtures, it appears that they are also experiencing reduced shrinkage. Even considering 95% confidence intervals, it can be seen that the SLWA mixture is a superior choice to NW-FA mixtures when it comes to achieving reduced shrinkage throughout the life cycle of the bridge deck topping mixture.

6.4 Compressive Creep Conclusions

Figure 47 shows the results of compressive creep tests performed during the course of the research project. The compressive creep values from the three NW-FA mixes have been averaged in order to compare against the compressive creep values obtained from testing the SLWA, Slag, and SLWA/Slag mixtures.

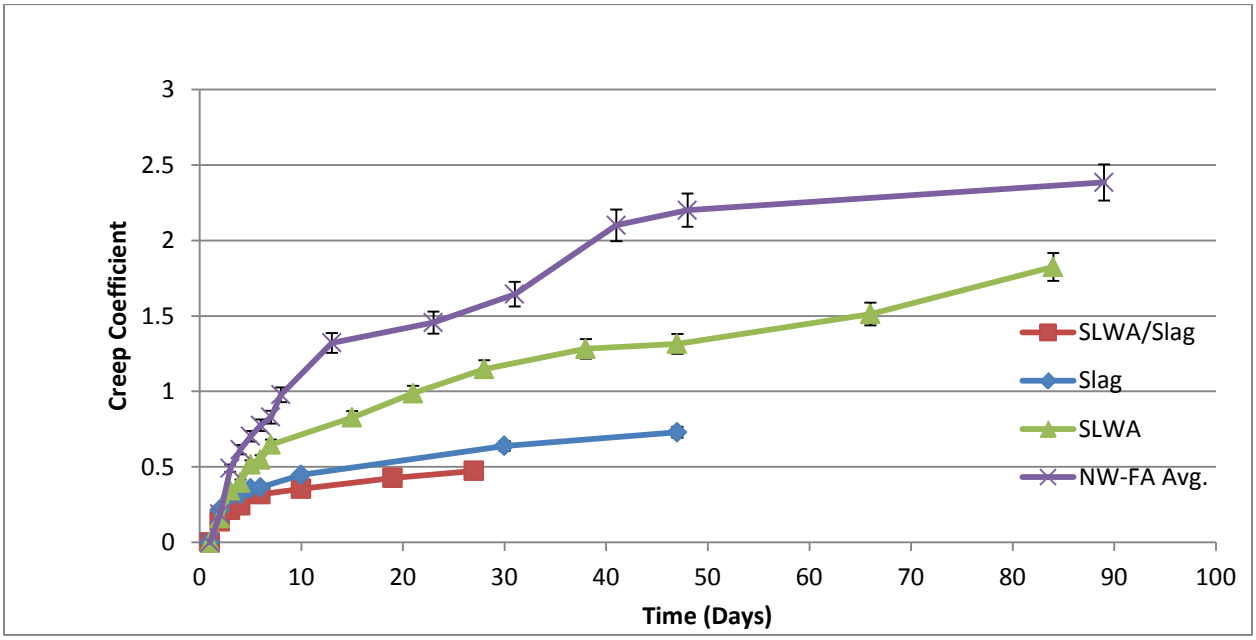

Figure 47 - Compressive Creep for NW-FA Avg. Vs. SLWA, Slag, and SLWA/Slag

It can be seen that the NW-FA mixtures experienced significantly more slag during their life cycles compared to the SLWA, Slag, and SLWA/Slag mixtures. As mentioned before, this can be attributed to the reduced drying shrinkage experienced by the SLWA, Slag, and SLWA/Slag mixtures compared to the NW-FA mixtures. This reduction in drying shrinkage led to a commensurate decrease in drying creep. Despite one of the goals of this research project being an increase in compressive creep, it will be shown below that the reduction in creep experienced by the SLWA, Slag, and SLWA/Slag mixtures is not a significant drawback.

6.5 Tensile Creep Conclusions

Figure 48 shows the results of tensile creep tests performed during the course of the research project. The tensile creep data from the SLWA mixture has been corrected to reflect the expected amount of elastic strain (30 με rather than 10 με).

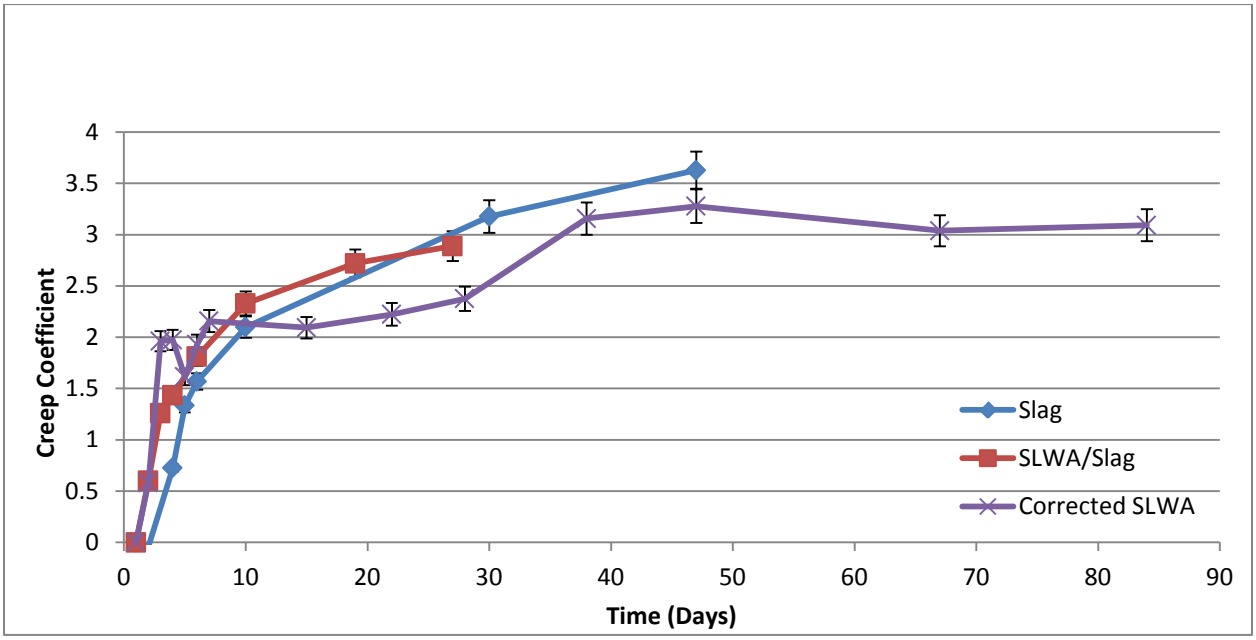

Figure 48: Tensile Creep Test Results

All three mixes display very similar values for tensile creep. Table 37 shows the values of tensile creep versus compressive creep.

Table 37 - Comparison between Compressive and Tensile Creep Values

Days	SLWA		Slag		SLWA/Slag	
	Comp.	Tensile	Comp.	Tensile	Comp.	Tensile
7	0.6	1.6	0.3	1.6	0.3	1.8
14	0.7	2.1	0.5	2.2	0.4	2.5
28	1.1	2.3	0.6	2.8	0.5	2.8
56	1.4	3.2	0.7	3.6	N/A	N/A
90	1.8	3.1	N/A	N/A	N/A	N/A

There are large differences between the values of compressive and tensile creep. The SLWA and SLWA/Slag mixtures experienced approximately 4-6 times more tensile creep than compressive creep for the ages which were tested. The SLWA values also showed large differences, approximately 2-3 times more tensile creep than compressive creep. These results

are not in agreement with the values reported by Poston in his report (Poston, Kesner et al. 1998). However, it is difficult to compare the results of this research project with the results reported by Poston since the test procedures were radically different.

6.6 Age Adjusted Effective Modulus Conclusions

Table 38 presents a comparison between the AAEM model stress profiles produced when comparing 90 day shrinkage and creep values between the SLWA and NW-FA mixtures. Table 36 values use the compressive creep values obtained via material testing. Note that to be precise, tensile creep values should be used (see Table 37). Compressive creep values are used in Table 36 in order to compare the SLWA and NW-FA mixtures more accurately since tensile creep values are not available for the NW-FA mixtures.

Table 38 - AAEM Stress Profile Comparison Between SLWA and NW-FA Mixtures W/Compressive Creep Values

Stress Profile (ksi) at Tapered Section, CIP Deck 7 in, Precast Girder 18 in.		
Stress Location	**SLWA 90 Day Test Results**	**NW-FA 90 Day Test Results**
Top of Deck	0.153	0.247
Bottom of Deck	0.373	0.457
Top of Girder	-0.475	-0.691
Bottom of Girder	0.285	0.418

The reduced shrinkage values experienced by the SLWA mixtures have a dramatic impact on the amount of tensile stress developed during a 90 curing cycle, reducing the stress at the top of deck by 38%.

Table 39 presents the results of AAEM modeling when comparing the stress values developed in the SLWA mixture to compressive creep versus tensile creep inputs. The values of compressive creep and tensile creep coefficients are 1.82 and 3.09, respectively.

Table 39 - AAEM Stress Profile Comparison Between SLWA w/Compressive Creep Values and SLWA W/Tensile Creep Values

Stress Profile (ksi) at Tapered Section, CIP Deck 7 in, Precast Girder 18 in.		
Stress Location	**SLWA 90 Day Compressive Creep**	**SLWA 90 Day Tensile Creep**
Top of Deck	0.153	0.16
Bottom of Deck	0.373	0.299
Top of Girder	-0.475	-0.417
Bottom of Girder	0.285	0.252

It can be seen that the increased tensile creep has very little effect on the amount of stress developed in the cross-section. These results are in agreement with the initial conclusion of the parametric study suggesting that increasing creep has little effect on reducing stress in the cross section, as the results of increasing creep by 70% did not result in a large reduction in stress experienced by the composite cross-section.

6.7 Economic Analysis

The factor that impacts the difference in cost between the NW-FA mixtures and mixtures utilized in this project is the cost of obtaining SLWA. See Table 38 for information regarding the increase in cost for using SLWA. Prices and shipping costs were obtained from Mr. Michael Robinson at the Carolina Stalite Company.

Table 40 - Economic Analysis for Addition of SLWA

Material	Cost (Including Shipping)	Amount Used Per Cubic Yard	Cost Per Cubic Yard of Concrete
Sand	$6.00/Ton	666 lb	$2.00
MS-16 SLWA	$79.00/Ton	403 lb	$15.90

When accounting for the amount of sand replaced by the SLWA, the increase in cost for adding SLWA to the mixture (including shipping costs) comes to $14.00 per cubic yard, which is an approximately 15% increase in price over a normal weight 4000 psi concrete mixture.

6.8 Mixture Selection

Table 41 presents a summary of the important parameters obtained from the material testing and data analysis performed during the course of this research project. NW-FA mixture averages are compared to SLWA mixture test results. Slag and SLWA/Slag are omitted due to incomplete test results at the current time.

Table 41 - Overall NW-FA Vs. SLWA Mixture Comparison

Property	NW-FA	SLWA
90 Day Shrinkage (με)	646	482
90 Day Creep Coefficient	2.4	1.82
28 Day Compressive Strength (PSI)	4000	3500
AAEM Stress (PSI) at top of deck	250	150
AAEM Stress (PSI) at bottom of deck	460	370

In conclusion, it can be seen that the SLWA mixture is superior to previously tested NW-FA mixtures for the purposes of reducing differential shrinkage in bridge deck topping mixtures. 90 day shrinkage values were reduced by 25%, which causes a 38% reduction in tensile stresses

due to differential shrinkage. Creep is similarly reduced from the NW-FA to SLWA mixtures. However, as shown previously, this reduction has little effect on the overall stresses developed during the 90 day curing cycle. Compressive strength is reduced from 4 ksi to 3.5 ksi; however, this reduction can be offset by a 40% replacement by weight of GGBFS for Portland cement. The SLWA mixture has been shown to out-perform the NW-FA mixtures previously tested in nearly every relevant category and it is the recommendation of the author that it be used in future bridge deck construction.

REFERENCES:

209, A. C. (2008). Guide for modeling and calculating shrinkage and creep in hardened concrete (ACI 209.2R-08), American Concrete Institute.

Bazant, Z. P. (1972). "Prediction of concrete creep effects using age-adjusted effective modulus method." ACI Journal **69**(4): 212-217.

Bissonnette, B. and M. Pigeon (1995). "Tensile creep at early ages of ordinary, silica fume and fiber reinforced concretes." Cement and Concrete Research **25**(5): 1075-1085.

Gilbert, R., et al. (2012). "Effects of shrinkage on the long-term stresses and deformations of composite concrete slabs." Engineering Structures **40**: 9-19.

Henkensiefken, R., et al. (2009). "Volume change and cracking in internally cured mixtures made with saturated lightweight aggregate under sealed and unsealed conditions." Cement and Concrete Composites **31**(7): 427-437.

Hooton, R. D., et al. (2004). The Effect of Ground, Granulated Blast Furnace Slag (Slag Cement) on the Drying Shrinkage of Concrete-A Critical Review of the Literature. Eighth CANMET/ACI International Conference on Fly Ash, Silica Fume, Slag and Natural Pozzolans in Concrete, Supplementary Papers Volume, American Concrete Institute.

Kosmatka, S. H., et al. (2002). Design and Control of Concrete Mixtures, 14th Edition, Portland Cement Association.

Li, B. X., et al. (2009). "Internal Curing of Saturated Lightweight Aggregate in High Performance Combined Concrete." Key Engineering Materials **405**: 212-218.

Mercer, M. (2012). Transverse Sub-Assemblage Testing of the Inverted-T Bridge System. Structural Engineering and Materials. Blacksburg, Virginia, Virginia Polytechnic and State University. **Master of Science**.

Mokarem, D. (2002). Development of Concrete Shrinkage Performance Specifications. Civil and Environmental Engineering. Blacksburg, Virginia, Virginia Polytechnic Institute and State University. **Doctor of Philosophy in Civil and Environmental Engineering:** 222.

Nahas, G., et al. (2008). Experimental study of uniaxial tensile creep of concrete. Creep, Shrinkage and Durability Mechanics of Concrete and Concrete Structures, Two Volume Set, Taylor & Francis**:** 453-457.

Østergaard, L., et al. (2001). "Tensile basic creep of early-age concrete under constant load." Cement and Concrete Research **31**(12): 1895-1899.

Pickett, G. (1942). The Effect of Chang in Moisture-Content on the Crepe of Concrete Under a Sustained Load. ACI Journal Proceedings, ACI.

Poston, R. W., et al. (1998). Performance criteria for concrete repair materials, Phase II laboratory results, DTIC Document.

Rossi, P., et al. (2013). "Comparison of concrete creep in tension and in compression: Influence of concrete age at loading and drying conditions." Cement and Concrete Research **51**(0): 78-84.

Schmitt, T. R. and D. Darwin (1999). "Effect of Material properties on Cracking in Bridge Decks." Journal of Bridge Engineering **4**(1): 8-13.

Silfwerbrand, J. (1997). "Stresses and strains in composite concrete beams subjected to differential shrinkage." ACI Structural Journal **94**(4).

Wang, S.-D., et al. (1995). "Alkali-activated slag cement and concrete: a review of properties and problems." Advances in cement research **7**(27): 93-102.

Wollmann, G. P., et al. (2003). "Creep and shrinkage effects in spliced prestressed concrete girder bridges." PCI journal **48**(6): 92-105.